

---

# TREE-BASED FORMALIZATION OF MULTI-AGENT COMPLEMENTARITY IN HUMAN–AI INTERACTIONS

---

Andrea Ferrario<sup>1,2,3</sup>

<sup>1</sup> Institute of Biomedical Ethics and History of Medicine, University of Zurich, Zurich, Switzerland

<sup>2</sup> SUPSI, Dalle Molle Institute for Artificial Intelligence (IDSIA), Lugano, Switzerland

<sup>3</sup> ETH Zurich, Zurich, Switzerland

June 4, 2026

## ABSTRACT

Complementarity is the case in which a human–AI interaction (HAI) outperforms the best prediction benchmark available among its members. Although this idea is central in human–AI interaction research, formal work on complementarity remains limited. Existing formal frameworks do not model how agents’ predictions compose into workflow-sensitive multi-agent protocols. We close this gap by introducing a tree-based formalization of complementarity in multi-agent HAI. An HAI protocol is represented by an ordered agent-role configuration together with a rooted planar binary tree whose leaves are decorated by prediction vectors. A local binary composition rule is evaluated recursively along the tree, yielding a tree-relative complementarity functional relative to a pointwise-min oracle benchmark. We prove four results. First, selector-based HAIs, including self- or AI-reliance, cannot achieve complementarity regardless of task, loss, or prediction quality. Second, in regression under squared loss, complementarity is equivalent to Euclidean distance minimization from the ground-truth vector; for  $N=2$ , the optimal linear-pooling weight has a closed form and a residual-correction interpretation. Third, under linear local composition, every protocol tree defines a barycentric coordinate chart on the simplex of leaf weights; Tamari-cover reparameterizations of protocol trees preserve complementarity, and for  $N=4$ , the Tamari-cover reparameterizations satisfy the pentagon identity. Fourth, in binary classification, no internal local composition can achieve complementarity with pointwise-min oracle benchmark under endpoint-monotone losses, including standard Bregman and many finite Bernoulli  $f$ -divergence losses; an analogous obstruction holds for coordinatewise-internal multiclass aggregation under cross-entropy. In summary, our framework shows that complementarity is attainable in multi-agent regression, but obstructed in classification under natural conditions on local aggregation and loss functions. If the pointwise-min oracle benchmark is appropriate for at least high-stakes HAI settings, this should prompt a revision of how complementarity is investigated empirically.

**Keywords:** Artificial Intelligence, Human–AI Interactions, Complementarity, Planar Binary Trees, Associahedra

## 1 Introduction

In 1998, the Dutch Eurodance project Alice Deejay rose to popularity by asking a relevant question: “Do you think you’re better off alone?”<sup>2</sup> Almost thirty years later, the human–AI interaction (HAI) domain answers *no*. The reason is that, under certain conditions, a human–AI team can perform better than the best standalone predictor available among its members. This phenomenon is called *complementarity*. While complementarity has attracted much attention across HAI [Bansal et al., 2021b,a, Hemmer et al., 2021, 2025, Donahue et al., 2022, Vaccaro et al., 2024], formal work on complementarity remains limited. Existing formalizations are centered on the two-agent setting: a human

---

\*Email: aferrario@ethz.ch.

<sup>2</sup>I refer to their song “Better off alone” for all details.

and an AI system interacting on the same prediction task. In this setting, complementarity compares the empirical loss of the human–AI team with the better aggregate empirical loss of the human and the AI considered separately [Hemmer et al., 2025, Donahue et al., 2022]. For instance, Donahue et al. [2022] analyze complementarity at the level of binary-classification loss ‘regimes’ in a two-agent setting while Rastogi et al. [2023] develop a taxonomy of human and ML strengths and an optimization framework for convex combinations of human and ML policies. Although complementarity is a central concept in HAI, the standard two-agent setting abstracts away from the structure of the interaction itself. Many real-world workflows involve more than one human and one AI system: experts and assistants may collaborate with AI tools in sequential decision processes; multiple human–AI dyads may contribute competing or complementary predictions; and several AI systems may aggregate, filter, or revise predictions at different stages of a workflow. Thus, once more than two agents are involved, complementarity requires specifying how agents are ordered, how local interactions are performed at the level of prediction vectors, and how intermediate outputs are composed into a final HAI protocol output.

We close this gap by developing a **tree-based formalization of complementarity in multi-agent HAI**. We study a regime in which all agents act on the same labeled dataset and predict the same target. A multi-agent HAI protocol is represented by an ordered agent-role configuration together with a rooted planar binary tree whose leaves are decorated by the agents’ prediction vectors. The ordered configuration captures the protocol-sensitive role order; the tree captures the binary compositions of the HAI protocol; and a local binary rule determines how two prediction vectors are combined at each internal node. Evaluating this rule recursively along the tree yields a tree-relative HAI protocol output.

Our contributions are as follows. First, we show a task-independent impossibility theorem for reliance. If local rules select one of their two inputs coordinatewise, such as in the case of self- and AI-reliance [Schemmer et al., 2023], then no interaction protocol can achieve complementarity relative to the pointwise-min oracle benchmark, regardless of the proportion of accurate reliance instances. Thus, *achieving complementarity requires producing interaction outputs that are not selected from the set of agent predictions*.

Second, we study regression under squared loss. In this setting, we prove that the complementarity functional has a geometric form: maximizing complementarity is equivalent to minimizing the Euclidean distance between the HAI protocol output and the ground-truth vector. For  $N = 2$  and linear aggregation, this yields a closed-form optimizer. Here, *complementarity depends on whether the human–AI disagreement direction corrects the AI residual with respect to ground truth, and whether the correction is large enough to place the optimum inside the feasible pooling segment*. For  $N \geq 3$ , we study complementarity invariance in relation to tree topology and interaction reparameterization.

Third, in regression with linear pooling as local composition and *any* loss function, we show that every tree defines a barycentric coordinate chart on the simplex of leaf weights. Using this coordinate representation, we prove complementarity invariance under Tamari covers of protocol trees [Tamari, 1962]. Therefore, *two distinct HAI protocol trees related by a Tamari move can lead to the same complementarity level after appropriately transporting their local parameters while keeping the same barycentric coordinates*. In addition, for  $N = 4$ , we prove a coherence result: the Tamari-cover reparameterizations satisfy the pentagon identity [Yanofsky, 2024].

Fourth, we show that in *binary classification, no internal local rule can achieve complementarity under endpoint-monotone losses*. Internal rules are those whose coordinatewise outputs remain between the corresponding input probabilities; endpoint monotonicity captures the basic requirement that assigning more probability to the true class should not increase loss. This impossibility result applies to broad families of Bregman and many standard finite Bernoulli  $f$ -divergence losses [Bregman, 1967, Ali and Silvey, 1966], including binary cross-entropy. The obstruction extends to multiclass problems with internal local rules under cross-entropy. We show that using non-internal rules, e.g., by amplifying binary logarithmic/logit pooling [Neyman and Roughgarden, 2023a], allows one to escape this impossibility regime.

In summary, our framework shows that complementarity is attainable in multi-agent regression, but obstructed in classification under natural conditions. If the pointwise-min oracle benchmark is appropriate for at least high-stakes HAI settings, this should prompt a revision of how complementarity is investigated empirically.

## 2 Related Work on Complementarity

In research on human–AI interaction, complementarity is the case in which the *human–AI team* performs better than either component alone [Bansal et al., 2021b,a, Hemmer et al., 2021, 2025]. This perspective shifted attention away from evaluating AI systems in isolation and toward the joint performance of the interaction, especially in advice-based decision-support settings where humans remain accountable for the final decision [Bansal et al., 2021b, Miller, 2023]. A central formalization is *complementarity team performance* (CTP), which treats complementarity as a binary property of a prediction-task human–AI interaction: complementarity is achieved whenever the empirical loss of the team is

strictly lower than the minimum of the empirical losses of the human and the AI considered separately [Hemmer et al., 2021, 2025]. In this sense, complementarity extends the selector logic characteristic of reliance relations, where the output is constrained to coincide with either the human or the AI prediction, by allowing interaction outputs that need not equal either input [Schemmer et al., 2023, Zhang et al., 2020, Bansal et al., 2021b].

Existing formal work focuses on the two-agent human–AI setting. Donahue et al. [2022] study complementarity in a two-component human–algorithm system directly in loss space. Their framework is developed for binary classification and partitions the input space into loss-homogeneous *regimes*. A regime is not an individual prediction on a sample, but a type or region of cases for which human, algorithmic, and combined performance can be summarized by loss rates. In regime  $i$ , the unaided human has loss  $h_i$ , the algorithm has loss  $a_i$ , and the combined system has loss  $c(a_i, h_i)$ , assumed to lie between the two standalone losses,  $\min\{a_i, h_i\} \leq c(a_i, h_i) \leq \max\{a_i, h_i\}$ . Complementarity is then defined relative to the better aggregate standalone loss, namely the better of the human and algorithm losses *after averaging across regimes*—see Def (1) in [Donahue et al., 2022]. Their impossibility results show that, in this regime-level loss framework, complementarity cannot be achieved if human and algorithm loss rates are constant over regimes or if one agent always weakly dominates the loss of the other—see Lemma 2 and 3 in [Donahue et al., 2022]. Rastogi et al. [2023] develop a taxonomy of human and ML strengths and weaknesses in decision-making, organized around task definition, input, internal processing, and output. They emphasize that complementarity should not be assumed because a human and an ML model are combined; rather, one should identify the concrete source of potential complementarity, such as access to different information, different objectives, different models of the world, or different output capabilities. To operationalize this idea, Rastogi et al. [2023] introduce an optimization framework in which a *joint policy* is obtained by convexly combining a human policy and an ML policy at the instance level. Their corresponding metrics of across-instance and within-instance complementarity quantify how the optimal joint policy distributes contribution across the two agents.

Furthermore, a related line of work has begun to study complementarity, deferral, and collaboration with multiple human experts. Hemmer et al. [2022] train a classifier together with an allocation system that routes each instance either to the model or to one of several human experts. Verma et al. [2023] study learning-to-defer with multiple experts, focusing on surrogate losses, calibration, and consistency guarantees for selecting which expert should handle a case. Paat and Shen [2025] use conformal prediction sets to select subsets of relevant human experts for instance-level classification. Finally, Peng et al. [2025] prove a no-free-lunch result for collaboration among two or more calibrated probabilistic agents in binary classification.

Taken together, these works show that complementarity depends on allocation, deferral, expert selection, and the distribution of expertise across agents. However, they do not provide a theory of complementarity as optimization over multi-agent interaction protocols. Their central design problem is typically which expert, model, or subset of experts to query, and whether a case should be deferred. By contrast, they do not model recursive prediction-vector composition conditional on real-world workflow topology. This limitation matters because many real-world HAI settings are not naturally two-agent interactions, and workflow structure can affect the final prediction. In medicine, for example, diagnostic and prognostic decisions may involve a general practitioner, a specialist, a radiologist, a nurse, a patient or caregiver, and one or more AI-based decision-support tools. In education, social services, or public administration, domain experts, case workers, lay users, and AI systems may all contribute different forms of information to a final judgment. In such settings, complementarity depends on which agents participate, on how human and artificial agents are ordered, which local interactions occur first, and how intermediate outputs are aggregated. Taken together, these considerations motivate the mathematical framework for complementarity that we introduce in what follows.

### 3 Tree-Based Formalization of Multi-Agent Complementarity

We introduce a tree-based formalism for empirical complementarity in multi-agent prediction-task HAIs. Our approach is as follows: (i) we distinguish HAIs, prediction-task HAIs, protocols, and protocol trees; (ii) we introduce notation for agents, roles, and ordered configurations; and (iii) we define tree-relative complementarity functionals.

#### 3.1 Human–AI Interactions, Agents, Roles, and Ordered Configurations

In what follows, a prediction task is a tuple  $\tau = (\mathcal{X}, \mathcal{Y}, \widehat{\mathcal{Y}}, \ell)$ , where  $\mathcal{X}$  is an input space,  $\mathcal{Y}$  is the label space,  $\widehat{\mathcal{Y}}$  is the prediction space, and  $\ell : \mathcal{Y} \times \widehat{\mathcal{Y}} \rightarrow [0, \infty)$ ,  $(y, \hat{y}) \mapsto \ell(y, \hat{y})$ , is a pointwise loss function. A labeled dataset is a finite set

$$D = \{(x_i, y_i)\}_{i=1}^n \subseteq \mathcal{X} \times \mathcal{Y}.$$

We use *human–AI interaction* (HAI) as a high-level term for a goal-oriented process in which human and AI agents contribute informational inputs that are integrated into a single output. In this paper we restrict attention to *prediction-task HAIs*: HAIs relative to a prediction task  $\tau = (\mathcal{X}, \mathcal{Y}, \widehat{\mathcal{Y}}, \ell)$ , in which the relevant inputs and outputs are prediction

vectors and the HAI output is evaluated against ground-truth labels in a dataset  $D$ . Thus, a prediction-task HAI specifies the agents—either human or AI systems—their roles, the prediction task, and the goal of producing an HAI output, but it does not yet determine how the agents interact. We call a *protocol* a concrete realization of such a prediction-task HAI: it specifies the order in which agent predictions enter the interaction, the local rules by which they are combined, and the way intermediate outputs are propagated to a final prediction. Hence, the same prediction-task HAI may admit several protocols. We elaborate on these concepts in what follows.

**Definition 1** (Agents, roles, and ordered configurations). *Let  $\mathcal{A} = \{a_1, \dots, a_N\}$  be a finite set of agents, let  $\mathcal{R}$  be a finite set of roles, and let  $r : \mathcal{A} \rightarrow \mathcal{R}$  be a function assigning a role to each agent. An ordered agent-role configuration is a tuple*

$$c_{\sigma, N} = ((a_{\sigma(1)}, r(a_{\sigma(1)})), \dots, (a_{\sigma(N)}, r(a_{\sigma(N)}))), \quad \sigma \in \mathfrak{S}_N,$$

where  $\mathfrak{S}_N$  denotes the permutation group on  $N$  elements.

For readability, in the discussion below we suppress agent identities and display only the ordered role sequence. In what follows, we assume all agents act on the same dataset  $D$  for the same prediction task  $\tau$ , and all agents predict the same target variable. Thus, each agent  $a_{\sigma(i)}$  in the configuration  $c_{\sigma, N}$  is represented by a predictor  $f_{a_{\sigma(i)}} : \mathcal{X} \rightarrow \hat{\mathcal{Y}}$ , with empirical prediction vector

$$\hat{y}^{(\sigma(i))} = (f_{a_{\sigma(i)}}(x_1), \dots, f_{a_{\sigma(i)}}(x_n)) \in \hat{\mathcal{Y}}^n.$$

Once  $\tau$  and  $D$  are fixed, we use the ordered configuration  $c_{\sigma, N}$  as the combinatorial representation of the HAI agents and roles. We now turn to HAI protocols. To address them, we introduce rooted planar binary trees.

**Definition 2** (Rooted planar binary trees). *Let  $\mathcal{Y}_N$  denote the set of rooted planar binary trees with  $N$  leaves, equivalently  $N - 1$  internal vertices. We use the recursive convention  $\mathcal{Y}_1 = \{|\}$ , where  $|$  is the one-leaf tree, with no internal vertex. For  $N \geq 2$ , define*

$$\mathcal{Y}_N = \coprod_{\substack{p+q=N \\ p, q \geq 1}} \{\sigma \vee \tau : \sigma \in \mathcal{Y}_p, \tau \in \mathcal{Y}_q\}.$$

Here  $\sigma \vee \tau$  denotes root grafting: a new internal root vertex is created whose left subtree is  $\sigma$  and whose right subtree is  $\tau$ . Thus every nontrivial rooted planar binary tree admits a unique decomposition into its left and right root subtrees.

For  $\mathbb{T} \in \mathcal{Y}_N$ , let  $V(\mathbb{T})$  denote its set of internal vertices. Then  $|V(\mathbb{T})| = N - 1$ . We define the left-to-right ordering  $o(\mathbb{T})$  of  $V(\mathbb{T})$  recursively. For the one-leaf tree,  $o(|) = \emptyset$ . If  $\mathbb{T} = \sigma \vee_x \tau$ , where  $x$  denotes the newly created root vertex, then

$$o(\mathbb{T}) = \{o(\sigma) < x < o(\tau)\}.$$

Equivalently, the internal vertices of the left subtree come first, then the root vertex  $x$ , and then the internal vertices of the right subtree.

The cardinality of  $\mathcal{Y}_N$  is the Catalan number  $|\mathcal{Y}_N| = C_{N-1} = \frac{1}{N} \binom{2N-2}{N-1}$ .

**Definition 3** (Protocol trees for a configuration). *Let  $c_{\sigma, N}$  be an ordered agent-role configuration of length  $N$ . A protocol tree for  $c_{\sigma, N}$  is a rooted planar binary tree  $\mathbb{T} \in \mathcal{Y}_N$  whose leaves are decorated from left to right by  $c_{\sigma, N}$ . Equivalently, once the predictors induced by  $c_{\sigma, N}$  are fixed, the leaves of  $\mathbb{T}$  are labeled from left to right by the corresponding ordered prediction vectors  $\hat{y}^{(\sigma(1))}, \dots, \hat{y}^{(\sigma(N))}$ .*

**Remark 1** (Examples of configurations). *Configurations with the same multiset of roles may still represent different HAIs because the order of the leaves is workflow-relevant. For  $N = 2$ , let  $A = \{a_1, a_2\}$  and  $r(a_1) = \text{expert}$ ,  $r(a_2) = \text{assistant}$  (both agents are human). Then  $c_{\sigma_1, 2} = (\text{expert}, \text{assistant})$ ,  $c_{\sigma_2, 2} = (\text{assistant}, \text{expert})$  are distinct configurations. For  $N = 3$ , let  $A = \{a_1, a_2, a_3\}$  and  $r(a_1) = \text{expert}$ ,  $r(a_2) = \text{assistant}$ , and  $r(a_3) = \text{AI system}$ . Examples such as*

$$c_{\sigma_1, 3} = (\text{expert}, \text{assistant}, \text{AI}), \quad c_{\sigma_2, 3} = (\text{assistant}, \text{AI}, \text{expert}), \quad c_{\sigma_3, 3} = (\text{expert}, \text{AI}, \text{assistant})$$

encode different interaction orders and therefore different protocols that correspond to different real-world workflows.

Throughout the paper, the ordered configuration  $c_{\sigma, N}$  is treated as fixed. Thus, we do not consider permutations of the leaves and we work with rooted planar binary trees because left-to-right leaf order is part of the workflow specification; in particular, mirror-related trees are not identified. For notational simplicity, once a configuration  $c_{\sigma, N}$  is specified, we write the ordered leaf predictions simply as

$$\hat{y}^{(1)}, \dots, \hat{y}^{(N)} \in \hat{\mathcal{Y}}^n.$$

## 3.2 Complementarity Functionals

### 3.2.1 The Two-Agent Setting

Following the literature on HAI, we introduce the complementarity functional in the two-agent setting.

**Definition 4** (Two-agent complementarity [Bansal et al., 2021b, Hemmer et al., 2025, Donahue et al., 2022]). *Let a human agent and an AI system interact in a HAI. Let  $\hat{y}^H = (\hat{y}_1^H, \dots, \hat{y}_n^H)$ ,  $\hat{y}^{AI} = (\hat{y}_1^{AI}, \dots, \hat{y}_n^{AI})$  denote the vectors of predictions of the human agent and the AI system over the dataset  $D$ . Let  $\hat{y}^{HAI} = (\hat{y}_1^{HAI}, \dots, \hat{y}_n^{HAI})$  denote the vector of ‘human–AI’ team predictions that results from the interaction between the human and the AI. These predictions depend on the inputs  $\hat{y}^H$  and  $\hat{y}^{AI}$ . Consider the average empirical losses*

$$L_{\clubsuit}(D) := \frac{1}{n} \sum_{i=1}^n \ell(y_i, \hat{y}_i^{\clubsuit}), \quad \clubsuit \in \{H, AI, HAI\}.$$

Define

$$\mathcal{C}_2(\hat{y}^H, \hat{y}^{AI}; D) := \min\{L_H(D), L_{AI}(D)\} - L_{HAI}(D). \quad (1)$$

The human–AI team achieves complementarity if

$$\mathcal{C}_2(\hat{y}^H, \hat{y}^{AI}; D) > 0.$$

Thus, complementarity records relative empirical gain between a human agent and an AI system by comparing the losses of the ‘human–AI team’ with those of the human and the AI system independently, on a given dataset. Our goal is to extend complementarity analysis from the two-agent setting to multi-agent protocols. Doing so, however, we start using a different  $N=2$  benchmark than (1). Specifically, we consider the functional at  $N=2$

$$\Psi(\hat{y}^H, \hat{y}^{AI}; D) = \frac{1}{n} \sum_{i=1}^n \min\{\ell(y_i, \hat{y}_i^H), \ell(y_i, \hat{y}_i^{AI})\} - \frac{1}{n} \sum_{i=1}^n \ell(y_i, \hat{y}_i^{HAI}). \quad (2)$$

The functional  $\Psi$  differs from  $\mathcal{C}_2$  in (1) by the placement of the minimum and the empirical average. The pointwise-min benchmark in (2) is the empirical counterpart of the population functional

$$\mathbb{E}_{X,Y}[\min\{\ell(Y, \hat{y}^H(X)), \ell(Y, \hat{y}^{AI}(X))\} - \ell(Y, \hat{y}^{HAI}(X))], \quad (3)$$

whereas the  $\mathcal{C}_2$  corresponds to the quantity

$$\min\{\mathbb{E}_{(X,Y)}[\ell(Y, \hat{y}^H(X))], \mathbb{E}_{(X,Y)}[\ell(Y, \hat{y}^{AI}(X))]\} - \mathbb{E}_{(X,Y)}[\ell(Y, \hat{y}^{HAI}(X))].$$

Thus,  $\Psi$  follows the standard statistical-learning passage from a pointwise population functional to its sample average. By contrast, the criterion in (1) places the minimum after aggregation: it compares aggregate risks, but it is not the empirical-risk analogue of the pointwise oracle-gain functional. They are related as follows:

**Proposition 1.** *For all predictions  $\hat{y}^H, \hat{y}^{AI}$  and every dataset  $D$*

$$\Psi(\hat{y}^H, \hat{y}^{AI}; D) \leq \mathcal{C}_2(\hat{y}^H, \hat{y}^{AI}; D). \quad (4)$$

*Proof.* Let  $a_i := \ell(y_i, \hat{y}_i^H)$ ,  $b_i := \ell(y_i, \hat{y}_i^{AI})$ . Averaging gives

$$\frac{1}{n} \sum_{i=1}^n \min\{a_i, b_i\} \leq \frac{1}{n} \sum_{i=1}^n a_i = L_H(D) \quad \text{and} \quad \frac{1}{n} \sum_{i=1}^n \min\{a_i, b_i\} \leq \frac{1}{n} \sum_{i=1}^n b_i = L_{AI}(D).$$

Therefore,  $\frac{1}{n} \sum_{i=1}^n \min\{a_i, b_i\} \leq \min\{L_H(D), L_{AI}(D)\}$ . Subtracting  $L_{HAI}(D)$  from both sides yields (4).  $\square$

Proposition 1 shows that the pointwise-min oracle benchmark is stricter than the classical aggregate benchmark in the two-agent complementarity case. The two benchmarks correspond to different reference risks. The classical benchmark compares the interaction output with the best fixed standalone predictor in aggregate, whereas the pointwise-min benchmark compares it with the best available standalone prediction at the case level before averaging.

### 3.2.2 The Multi-Agent Setting

We now move to the complementarity functional for  $N \geq 2$  generalizing the case  $N = 2$ . We start with a structural assumption:

**Assumption 1** (Benchmark–interaction decomposition). *Complementarity functionals have the form*

$$\Psi(\hat{y}^{(1)}, \dots, \hat{y}^{(N)}; D) = \Phi(\hat{y}^{(1)}, \dots, \hat{y}^{(N)}; D) - \Theta(\hat{y}^{(1)}, \dots, \hat{y}^{(N)}; D),$$

where  $\Phi$  is a benchmark term independent of protocol topology, and  $\Theta$  is the loss of the protocol output.

This assumption generalizes the structure of the complementarity functional in Definition 1 to the multi-agent setting. Then, the problem becomes to (1) choose the benchmark term  $\Phi$ , and (2) introduce the interaction term  $\Theta$ . The benchmark term can be introduced by generalizing  $\Psi$  in (2). To address the interaction part, however, we need to introduce the logic according to which agents are allowed to interact in an HAI. The focus on planar binary trees reveals a natural simplification: local *binary* interactions. On this view, HAIs evolve through elementary interaction steps, each involving two inputs at a time, with intermediate outputs then propagated through the interaction protocol. The binary restriction gives a direct generalization of the standard  $N = 2$  human–AI setting: every local interaction is still a two-input interaction, but larger protocols can be built by composing such elementary steps. This covers natural sequential workflows, such as expert–assistant–AI configurations, deferred referral structures, and settings in which several human–AI dyads are combined into a final decision. Further, it separates local interaction from global protocol structure. The same local rule can be evaluated on different trees, allowing us to ask whether complementarity depends on the local aggregation mechanism or on the order in which agents enter the workflow. Finally, although the binary restriction is a simplification as some workflows may involve simultaneous or higher-arity interactions, it yields a mathematically tractable class of protocols: binary trees expose algebraic questions about associativity, geometric questions about attainable prediction regions, and analytical questions about optimizing complementarity under a chosen loss. Thus, we arrive at:

**Assumption 2** (Local binary composition). *Let  $\mathbb{T} \in \mathbb{Y}_N$  with leaves labeled by  $\hat{y}^{(1)}, \dots, \hat{y}^{(N)} \in \hat{\mathcal{Y}}^n$ . Its output*

$$\hat{y}_{\mathbb{T}} := m_{\mathbb{T}}(\hat{y}^{(1)}, \dots, \hat{y}^{(N)}) \in \hat{\mathcal{Y}}^n$$

is defined recursively by applying a local binary rule  $m_2 : \hat{\mathcal{Y}}^n \times \hat{\mathcal{Y}}^n \rightarrow \hat{\mathcal{Y}}^n$  at each internal node of  $\mathbb{T}$ .

We introduce the complementarity functional for interactions with  $N \geq 2$  agents using our tree-based formulation. It is the main mathematical object of this work.

**Definition 5** (Tree-relative complementarity functional). *Let  $\tau = (\mathcal{X}, \mathcal{Y}, \hat{\mathcal{Y}}, \ell)$  be a prediction task and  $D = \{(x_i, y_i)\}_{i=1}^n$  be a labeled dataset. Let  $m_2$  be a local binary composition rule and  $\hat{y}^{(1)}, \dots, \hat{y}^{(N)}$  be the  $N$  predictions of  $N$  agents of a configuration  $c_{\sigma, N}$ .*

For any protocol tree  $\mathbb{T} \in \mathbb{Y}_N$  for  $c_{\sigma, N}$ , the tree-relative complementarity functional  $\Psi_{\mathbb{T}}^{m_{\mathbb{T}}}$  is defined as

$$\Psi_{\mathbb{T}}^{m_{\mathbb{T}}}(\hat{y}^{(1)}, \dots, \hat{y}^{(N)}; D) := \Phi(\hat{y}^{(1)}, \dots, \hat{y}^{(N)}; D) - \Theta_{\mathbb{T}}(\hat{y}^{(1)}, \dots, \hat{y}^{(N)}; D), \quad (5)$$

where the multi-agent benchmark term is the pointwise-min

$$\Phi(\hat{y}^{(1)}, \dots, \hat{y}^{(N)}; D) := \frac{1}{n} \sum_{i=1}^n \min_{1 \leq j \leq N} \ell(y_i, \hat{y}_i^{(j)}). \quad (6)$$

and the interaction term reads

$$\Theta_{\mathbb{T}}(\hat{y}^{(1)}, \dots, \hat{y}^{(N)}; D) := \frac{1}{n} \sum_{i=1}^n \ell(y_i, \hat{y}_i^{\mathbb{T}}). \quad (7)$$

### 3.2.3 On the Choice of Benchmark in the Definition of Complementarity

The comparison in Proposition 1 extends to the  $N$ -agent tree-relative setting. For each leaf prediction, let  $L_j(D) := \frac{1}{n} \sum_{i=1}^n \ell(y_i, \hat{y}_i^{(j)})$ ,  $j = 1, \dots, N$ . If one generalizes the classical aggregate complementarity criterion to  $N$  agents by defining

$$\mathcal{C}_{N, \mathbb{T}}^{m_{\mathbb{T}}}(\hat{y}^{(1)}, \dots, \hat{y}^{(N)}; D) := \min_{1 \leq j \leq N} L_j(D) - \Theta_{\mathbb{T}}(\hat{y}^{(1)}, \dots, \hat{y}^{(N)}; D), \quad (8)$$

with the same interaction term  $\Theta_{\mathbb{T}}$  as in (7), then  $\Psi_{\mathbb{T}}^{m_{\mathbb{T}}}(\hat{y}^{(1)}, \dots, \hat{y}^{(N)}; D) \leq \mathcal{C}_{N, \mathbb{T}}^{m_{\mathbb{T}}}(\hat{y}^{(1)}, \dots, \hat{y}^{(N)}; D)$ .

The two complementarity functionals coincide if and only if at least one fixed agent is pointwise loss-minimal on every sample in  $D$ , that is

$$\exists \bar{j} \in \{1, \dots, N\} : \ell(y_i, \hat{y}_i^{(\bar{j})}) = \min_{1 \leq j \leq N} \ell(y_i, \hat{y}_i^{(j)}) \quad \text{for every } i = 1, \dots, n.$$

This comparison clarifies the benchmark used throughout the paper. Let  $\mathcal{F}_N = \{f_1, \dots, f_N\}$  denote the finite family of available agent predictors, and let  $f_\top$  denote the predictor induced by the protocol tree  $\top$ . Its population risk is

$$R(f_\top) := \mathbb{E}_{(X,Y)}[\ell(Y, f_\top(X))].$$

At the population level, the classical aggregate benchmark corresponds to the best fixed member of  $\mathcal{F}_N$  in expected risk:

$$R_C(\mathcal{F}_N) := \min_{1 \leq j \leq N} \mathbb{E}_{(X,Y)}[\ell(Y, f_j(X))].$$

The pointwise-min benchmark corresponds instead to the finite-family pointwise oracle:

$$R_{\text{pw}}(\mathcal{F}_N) := \mathbb{E}_{(X,Y)} \left[ \min_{1 \leq j \leq N} \ell(Y, f_j(X)) \right].$$

Thus, at the population level, *complementarity can be understood as minus an excess risk relative to the chosen benchmark*. The empirical counterparts of both complementarity functionals are obtained by the usual plug-in passage from population risk to empirical risk. Both benchmarks are legitimate, but they answer different questions. The aggregate benchmark in (8) asks whether the interaction improves over deploying the best fixed component across all cases. The pointwise-min benchmark (6) in (5) asks whether the protocol improves over the best available prediction at the case level, before averaging, instead.

This distinction is relevant for HAI research because the aggregate benchmark can report complementarity even when the interaction fails to improve over the best available prediction on each case. Consider two agents,  $H$  and  $A$ , and losses in arbitrary units:

	$L_H$	$L_A$	$L_{\text{HAI}}$
case 1	0	4	1
case 2	4	0	1

Hence  $C_2 = 2 - 1 = 1 > 0$ ,  $\Psi = 0 - 1 = -1 < 0$ . Thus, the aggregate benchmark reports complementarity, while the pointwise-min benchmark detects that the protocol is worse than an available prediction on every case. A second example separates complementarity from casewise selection. Suppose the protocol selects the better available prediction on each case, again with losses in arbitrary units:

	$L_H$	$L_A$	$L_{\text{HAI}}$
case 1	0	4	0
case 2	4	0	0

Then  $C_2 = 2 - 0 = 2 > 0$ ,  $\Psi = 0 - 0 = 0$ . The aggregate benchmark treats the casewise selector as complementary relative to the best fixed agent. The pointwise-min benchmark classifies it as optimal selection among available predictions, but not as improvement beyond the best available prediction. (This is a case of ‘appropriate reliance,’ as discussed in Section 4.2.)

For this reason, *the pointwise-min benchmark is useful in workflows where case-level errors matter*. Examples include medical diagnosis, triage, and review, judicial or administrative decision support, and safety-critical model monitoring. The same consideration applies to multi-AI and AI-agent environments, where several models, model versions, systems, or agents may produce predictions for the same case. In such settings, an aggregate benchmark may show that an ensemble or multi-agent protocol improves over the best fixed model on average, while still failing to use the best available prediction on important cases. The pointwise-min benchmark is stricter because it evaluates the protocol against the best available casewise prediction from the finite family. In lower-stakes or large-scale settings where the relevant deployment alternative is a single fixed component and the primary object of evaluation is average performance, the aggregate benchmark may be sufficient, although it can inflate complementarity by ignoring casewise heterogeneity among agents. Unless explicitly stated otherwise, *all complementarity claims in the remainder of the paper are relative to pointwise-min oracle benchmarks—see eq. 6*.

This benchmark choice matters for the interpretation of the impossibility results below—see Sections 4.2 and 8.1. These results use the pointwise-min benchmark. By contrast, the regression optimization results are largely insensitive to the benchmark choice—see Sections 5, 6, and 7. In squared-loss regression, replacing the pointwise-min benchmark by the aggregate benchmark changes the complementarity functional only by an additive constant independent of the protocol output. Thus the optimizer, protocol-indifference loci, and tree-reparameterization invariance results remain unchanged; only the numerical complementarity value, and hence the threshold for strict positivity, changes.

### 3.3 Optimizing Tree-Relative Complementarity Functionals

The tree-relative complementarity functional  $\Psi_{\mathbb{T}}^{m_{\mathbb{T}}}$  supports several optimization regimes, depending on which part of the interaction design is treated as fixed and which part is treated as variable. While in this paper we work with a fixed ordered configuration and identify the corresponding decorated protocol set with  $Y_N$  to keep notation light, in applications, additional workflow constraints  $\mathbf{c}$  may exclude some tree shapes. In that case one replaces  $Y_N$  by an admissible subset  $Y_N^{\text{adm}}(\mathbf{c}) \subseteq Y_N$ . We distinguish two optimization cases.

**Case 1: tree optimization for fixed local interaction.** Fix a local rule  $m_2$ . The optimization problem is

$$\mathbb{T}^* \in \arg \max_{\mathbb{T} \in Y_N} \Psi_{\mathbb{T}}^{m_{\mathbb{T}}}(\hat{y}^{(1)}, \dots, \hat{y}^{(N)}; D). \quad (9)$$

This is the pure protocol-topology problem: one searches only over rooted planar binary trees.

**Case 2: joint optimization over trees and local rules.** Let  $\mathcal{M}$  be a class of admissible local rules, possibly parametric. For a fixed tree  $\mathbb{T} \in Y_N$ , choose an assignment

$$\mathbf{m}_{\mathbb{T}} = (m_{2,v})_{v \in V(\mathbb{T})} \in \mathcal{M}^{N-1}$$

of local rules to the  $N - 1$  internal nodes of  $\mathbb{T}$ . This assignment induces, by recursive evaluation along  $\mathbb{T}$ , a tree-level composition map  $m_{\mathbb{T}}$ . The dependence of  $m_{\mathbb{T}}$  on the node-wise assignment  $\mathbf{m}_{\mathbb{T}}$ , and on any node-wise parameters when  $\mathcal{M}$  is parametric, is suppressed unless it is needed explicitly. One may then optimize jointly over protocol topology and local interaction:

$$\sup_{\mathbb{T} \in Y_N, \mathbf{m}_{\mathbb{T}} \in \mathcal{M}^{N-1}} \Psi_{\mathbb{T}}^{m_{\mathbb{T}}}(\hat{y}^{(1)}, \dots, \hat{y}^{(N)}; D). \quad (10)$$

This regime treats both the tree and the local aggregation mechanism as design variables. If  $\mathcal{M}$  is parametric, the same family of local rules may be used at every internal node, while the parameter values may vary from node to node.

## 4 Local Compositions and a First Impossibility Result

In this section, we discuss some properties of local binary compositions and show a first impossibility result.

### 4.1 Local Compositions and Associativity

Let us introduce two families  $\mathcal{M}_{sel}$  and  $\mathcal{M}_{\rho}$  of local binary compositions. Elements of  $\mathcal{M}_{sel}$  are *selectors*, namely, set-theoretic local binary compositions that return one of their inputs coordinatewise on ordered sets. Examples are  $m_2(u, v) = u$ ,  $m_2(u, v) = v$ ,  $m_2(u, v) = \min\{u, v\}$ , and  $m_2(u, v) = \max\{u, v\}$ . Elements of  $\mathcal{M}_{\rho}$  are *quasi-arithmetic means*  $m_{2,\alpha}^{\rho}$  [Kolmogorov, 1930, Nagumo, 1930], with  $\alpha \in [0, 1]$ . Let  $\rho : I \rightarrow \mathbb{R}$  be continuous and strictly monotone increasing, where  $I \subseteq \mathbb{R}$  is an interval. For  $\alpha \in [0, 1]$ , define the coordinatewise local rule

$$(m_{2,\alpha}^{\rho}(u, v))_i := \rho^{-1}(\alpha\rho(u_i) + (1 - \alpha)\rho(v_i)), \quad (11)$$

for  $u, v \in I^n$ . If  $\rho = \text{id}$ , one obtains the family of *linear pooling* functions  $\alpha u + (1 - \alpha)v$ . If  $I = (0, 1)$  and  $\rho = \text{logit}$ , that is  $\rho(p) = \log\left(\frac{p}{1-p}\right)$ ,  $p \in (0, 1)$ , one obtains *logit pooling* functions. Thus quasi-arithmetic means provide local compositions for both regression-style and probabilistic aggregation rules. While the four examples of selector compositions are associative, quasi-arithmetic means are non-associative except in the projection cases:

**Lemma 1.** *The quasi-arithmetic mean  $m_{2,\alpha}^{\rho}$  in (11) is associative if and only if  $\alpha \in \{0, 1\}$ .*

*Proof.* Let  $I$  contain at least two points. For all  $u, v, w \in I$ ,  $m_{2,\alpha}^{\rho}(m_{2,\alpha}^{\rho}(u, v), w) = m_{2,\alpha}^{\rho}(u, m_{2,\alpha}^{\rho}(v, w))$  is equivalent to  $\alpha^2 = \alpha$ ,  $(1 - \alpha) = (1 - \alpha)^2$ . Then  $\alpha \in \{0, 1\}$ .  $\square$

While selector compositions collapse tree dependence, Lemma 1 shows that within the quasi-arithmetic family, every nontrivial weight choice  $\alpha \in (0, 1)$  yields a non-associative local rule. Hence, in that family, tree topology becomes a source of variation for complementarity.

## 4.2 Reliance Never Reaches Complementarity

We call *reliance* the selector-based special case of a prediction-task HAI. In the standard two-agent decision-support setting, the inputs are the human and AI predictions  $\hat{y}_i^H$  and  $\hat{y}_i^{AI}$  for the same case  $i$ . Reliance occurs when the interaction output is not a transformed or combined prediction, but simply one of these two inputs: if  $\hat{y}_i^{HAI} = \hat{y}_i^H$ , the case is one of *self-reliance*; if  $\hat{y}_i^{HAI} = \hat{y}_i^{AI}$ , it is one of *AI reliance* [Schemmer et al., 2023, Zhang et al., 2020, Ferrario, 2025]. In the HAI literature, the normative target is often *appropriate reliance*: the human follows correct AI advice when the AI is right and ignores it when the AI is wrong. This casewise notion extends to datasets: a two-agent HAI exhibits reliance on  $D$  if, for every sample in  $D$ , its output is either the human prediction or the AI prediction. Then one may measure appropriate reliance on  $D$  by the proportion of samples on which the selected source is correct. However, the theorem below shows that selector local rules do not yield complementarity in multi-agent HAIs.

**Theorem 1** (Selectors cannot yield complementarity). *Let  $\mathsf{T} \in \mathcal{Y}_N$ , and suppose the local rule  $m_2 \in \mathcal{M}_{sel}$ :  $(m_2(u, v))_i \in \{u_i, v_i\}$  for all  $u, v \in \hat{\mathcal{Y}}^n$ ,  $i = 1, \dots, n$ . Then, for every dataset  $D$ ,  $\Psi_{\mathsf{T}}^{m_2}(\hat{y}^{(1)}, \dots, \hat{y}^{(N)}; D) \leq 0$ .*

*Proof.* Fix a case  $i$ . Since  $m_2$  selects one of its two coordinate inputs, recursive composition along the tree implies that the protocol output on coordinate  $i$  equals one of the leaf predictions:  $(m_{\mathsf{T}}(\hat{y}^{(1)}, \dots, \hat{y}^{(N)}))_i \in \{\hat{y}_i^{(1)}, \dots, \hat{y}_i^{(N)}\}$ . Hence

$$\min_{1 \leq j \leq N} \ell(y_i, \hat{y}_i^{(j)}) \leq \ell(y_i, (m_{\mathsf{T}}(\hat{y}^{(1)}, \dots, \hat{y}^{(N)}))_i).$$

Averaging over  $i = 1, \dots, n$  yields

$$\Phi(\hat{y}^{(1)}, \dots, \hat{y}^{(N)}; D) \leq \frac{1}{n} \sum_{i=1}^n \ell(y_i, (m_{\mathsf{T}}(\hat{y}^{(1)}, \dots, \hat{y}^{(N)}))_i) \iff \Psi_{\mathsf{T}}^{m_2}(\hat{y}^{(1)}, \dots, \hat{y}^{(N)}; D) \leq 0. \quad \square$$

**Corollary 1.** *Consider the two-agent configuration (human, AI). If their interaction output exhibits self-reliance or AI reliance on every sample of  $D$ , then the HAI cannot achieve complementarity, regardless of the proportion of appropriately reliant cases on  $D$ .*

## 5 Complementarity in Regression Under Squared Loss

We now turn to regression, showing that tree-relative complementarity functional optimization under squared loss admits a geometric interpretation and can be solved analytically in a few cases. The label and prediction spaces are  $\mathcal{Y} = \hat{\mathcal{Y}} = \mathbb{R}$ , so prediction vectors lie in  $\hat{\mathcal{Y}}^n = \mathbb{R}^n$  and the loss is the squared loss, i.e.,  $\ell(y, \hat{y}) = (y - \hat{y})^2$ .

**Proposition 2** (Squared-loss complementarity as distance minimization). *Assume regression with squared loss. Define*

$$K_n := \frac{1}{n} \sum_{i=1}^n \min_{1 \leq j \leq N} (y_i - \hat{y}_i^{(j)})^2. \quad (12)$$

*Then, for every tree  $\mathsf{T} \in \mathcal{Y}_N$  and every induced output  $\hat{y}_{\mathsf{T}} \in \hat{\mathcal{Y}}^n$ ,*

$$n\Psi_{\mathsf{T}}^{m_2}(\hat{y}^{(1)}, \dots, \hat{y}^{(N)}; D) = nK_n - \|y - \hat{y}_{\mathsf{T}}\|_2^2, \quad (13)$$

*where  $\|x\|_2^2 = \sum_{i=1}^n x_i^2$ ,  $x \in \mathbb{R}^n$ . Hence, for fixed  $D$  and fixed leaf predictions, maximizing complementarity is equivalent to minimizing the Euclidean distance between the root output  $\hat{y}_{\mathsf{T}}$  and the label vector  $y$ .*

*Proof.* Eq. (13) follows from the definition of the tree-relative complementarity functional in eq. (7) and the squared loss.  $\square$

It follows from Proposition 2 that  $\Psi_{\mathsf{T}}^{m_2} > 0 \iff \|y - \hat{y}_{\mathsf{T}}\|_2^2 < nK_n$ . Thus complementarity holds exactly when the tree prediction  $\hat{y}_{\mathsf{T}}$  lies inside the Euclidean sphere centered at  $y$  with radius  $\sqrt{nK_n}$ . Likewise,  $\Psi_{\mathsf{T}}^{m_2} = 0$  occurs exactly when  $\hat{y}_{\mathsf{T}}$  lies on that sphere as displayed in Figure 1. Note that, by definition,  $K_n = \Phi(\hat{y}^{(1)}, \dots, \hat{y}^{(N)}; D)$ —see eq. (6).

Further, in regression under the squared loss function, *complementarity invariance under HAI protocol change* has a direct geometric interpretation. By Proposition 2, two distinct trees  $\mathsf{T}, \mathsf{T}' \in \mathcal{Y}_N$  have the same complementarity value

$$\Psi_{\mathsf{T}}^{m_2}(\hat{y}^{(1)}, \dots, \hat{y}^{(N)}; D) = \Psi_{\mathsf{T}'}^{m_2}(\hat{y}^{(1)}, \dots, \hat{y}^{(N)}; D) \iff \|y - \hat{y}_{\mathsf{T}}\|_2^2 = \|y - \hat{y}_{\mathsf{T}'}\|_2^2. \quad (14)$$

Geometrically, (14) holds when the two protocol outputs  $\hat{y}_{\mathsf{T}}$  and  $\hat{y}_{\mathsf{T}'}$  lie on the same sphere centered at  $y$ . Thus, equality of complementarity values does not require equality of protocol outputs: two distinct protocols of the same HAI may achieve the same level of complementarity while producing different predictions. Under linear pooling, the parameter values for which this protocol-indifference condition holds form an algebraic locus:

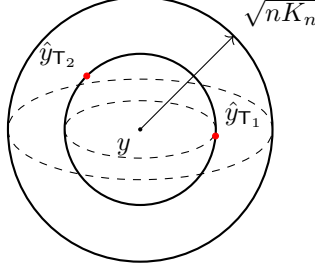


Figure 1: Geometric interpretation of complementarity in regression under squared loss in  $\mathbb{R}^n$ . The outer sphere is centered at the ground-truth vector  $y$  and has radius  $\sqrt{nK_n}$ , corresponding to the boundary  $\|y - \hat{y}_T\|_2^2 = nK_n$ , i.e., zero complementarity. The smaller concentric sphere represents a lower common squared distance from  $y$ ; the points  $\hat{y}_{T_1}$  and  $\hat{y}_{T_2}$  illustrate two protocol outputs with the same positive complementarity value.

**Proposition 3** (Protocol-indifference locus under linear pooling). *Assume regression under squared loss and fix leaf predictions  $\hat{y}^{(1)}, \dots, \hat{y}^{(N)} \in \mathbb{R}^n$ . Let  $T, T' \in \mathcal{Y}_N$ . For each tree, fix the canonical recursive left-to-right ordering of its  $N - 1$  internal nodes and assign the local linear-pooling rule*

$$m_{2, \alpha_k}^{\text{id}}(u, v) = \alpha_k u + (1 - \alpha_k)v$$

*to the  $k$ -th internal node. For  $\alpha = (\alpha_1, \dots, \alpha_{N-1}) \in [0, 1]^{N-1}$ , write  $\hat{y}_T(\alpha)$  and  $\hat{y}_{T'}(\alpha)$  for the corresponding root outputs.*

*Then the set of local weights for which the two protocol trees have the same complementarity value is*

$$\mathcal{S}_{T, T'} := \{\alpha \in [0, 1]^{N-1} : P_{T, T'}(\alpha) = 0\},$$

*where*

$$P_{T, T'}(\alpha) := \|y - \hat{y}_T(\alpha)\|_2^2 - \|y - \hat{y}_{T'}(\alpha)\|_2^2.$$

*Moreover,  $P_{T, T'}$  is a polynomial in  $\alpha$  of degree at most  $2(N - 1)$ . The protocol-indifference locus is nonempty: it always contains the two corners*

$$(0, \dots, 0) \quad \text{and} \quad (1, \dots, 1).$$

*Proof.* The benchmark term  $\Phi$  is independent of the protocol tree. Hence two trees have the same complementarity value if and only if their squared-loss interaction terms are equal, equivalently  $P_{T, T'}(\alpha) = 0$ . For linear local composition, each coordinate of  $\hat{y}_T(\alpha)$  and  $\hat{y}_{T'}(\alpha)$  is a polynomial in  $\alpha$  of degree at most  $N - 1$ , since each leaf contribution is weighted by a product of local weights along a root-to-leaf path. Therefore each squared norm has degree at most  $2(N - 1)$ , and so does  $P_{T, T'}$ . Finally, if  $\alpha = (1, \dots, 1)$ , every internal node selects its left input, so every tree outputs the leftmost leaf prediction  $\hat{y}^{(1)}$ . If  $\alpha = (0, \dots, 0)$ , every internal node selects its right input, so every tree outputs the rightmost leaf prediction  $\hat{y}^{(N)}$ . Hence both corners belong to  $\mathcal{S}_{T, T'}$ .  $\square$

We now study complementarity in regression under squared loss in low- $N$  cases.

### 5.1 The $N = 2$ Case and Complementarity Maximization

Let  $N = 2$  and  $m_{2, \alpha}^{\text{id}} \in \mathcal{M}_{\text{id}}$ , that is  $m_{2, \alpha}^{\text{id}}(u, v) = \alpha u + (1 - \alpha)v, \alpha \in [0, 1]$ . We choose the agent configuration (human, AI) to decorate the leaves of the unique tree  $T \in \mathcal{Y}_2$ —see Figure 2. The case (AI, human) is treated analogously; results are interpreted under the new agent order.

**Proposition 4** (Maximizing complementarity for  $N = 2$  regression under squared loss and linear pooling). *Let  $T$  be the unique tree in  $\mathcal{Y}_2$ . Choose the squared loss and let*

$$m_{2, \alpha}^{\text{id}}(u, v) = \alpha u + (1 - \alpha)v, \quad \alpha \in [0, 1].$$

*Then*

$$n\Psi_T^{m_{2, \alpha}^{\text{id}}}(\hat{y}^H, \hat{y}^{AI}; D) = -A_n \alpha^2 - 2B_n \alpha + (nK_n - C_n), \quad (15)$$

*where*

$$A_n = \|\hat{y}^H - \hat{y}^{AI}\|_2^2, \quad B_n = \langle \hat{y}^H - \hat{y}^{AI}, \hat{y}^{AI} - y \rangle, \quad C_n = \|\hat{y}^{AI} - y\|_2^2.$$

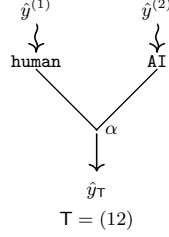


Figure 2: The rooted planar binary tree for  $N = 2$ , with leaves decorated by human and AI roles, the corresponding prediction vectors  $\hat{y}^{(1)}$  and  $\hat{y}^{(2)}$ .  $\hat{y}_T$  is the tree output.

If  $A_n > 0$ , the maximizing weight is

$$\alpha^* = \Pi_{[0,1]} \left( -\frac{B_n}{A_n} \right).$$

If  $A_n = 0$ , the aggregate is constant in  $\alpha$  and yields no complementarity.

*Proof.* Appendix A. □

Proposition 4 admits an explicit geometric interpretation. Let us rewrite  $B_n$  as  $B_n = \|\hat{y}^H - \hat{y}^{AI}\|_2 \|\hat{y}^{AI} - y\|_2 \cos \theta$ . Then, the interior case  $-\frac{B_n}{A_n} \in (0, 1)$  is equivalent to the two inequalities

$$\cos \theta < 0 \quad \text{and} \quad \frac{\|\hat{y}^H - \hat{y}^{AI}\|_2}{\|\hat{y}^{AI} - y\|_2} > -\cos \theta. \quad (16)$$

The first condition says that the human–AI disagreement direction  $\hat{y}^H - \hat{y}^{AI}$  has a component pointing *against* the AI residual  $\hat{y}^{AI} - y$ . The second condition says that the human prediction  $\hat{y}^H$  moves sufficiently far in that corrective direction for the projection of  $y$  onto the human–AI line  $\hat{y}^H - \hat{y}^{AI}$  to lie inside the convex segment between  $\hat{y}^{AI}$  and  $\hat{y}^H$ .

**Corollary 2.** *In the interior case  $-\frac{B_n}{A_n} \in (0, 1)$ , the optimized value of the complementarity functional is*

$$n\Psi_T^{m_{2,\alpha^*}^{\text{id}}}(\hat{y}^H, \hat{y}^{AI}; D) = nK_n - C_n + \frac{B_n^2}{A_n} = nK_n - \|\hat{y}^{AI} - y\|_2^2 \sin^2 \theta, \quad (17)$$

where  $\alpha^* \in (0, 1)$ . Thus, linear pooling can remove only the component of the AI residual that lies along the human–AI disagreement direction. In particular, conditional on a fixed pointwise-oracle benchmark  $K_n$  and a fixed AI residual norm  $\|\hat{y}^{AI} - y\|_2$ , the optimized complementarity value is maximized by minimizing  $\sin^2 \theta$ , which occurs when the human–AI disagreement direction is opposite to the AI residual.

### 5.1.1 Numerical illustration of the $N = 2$ regression case

We illustrate the  $N = 2$  regression case with linear pooling by training a random-forest regressor on the California housing training set and evaluating complementarity on the test set. All details on the experimental setting are in Appendix E. Taking the AI residual  $r = \hat{y}^{AI} - y$  as fixed, we generate synthetic human predictions of the form  $\hat{y}^H = \hat{y}^{AI} + d$ , where the displacement  $d$  has controlled angle  $\theta$  with  $r$  and controlled norm ratio  $q = \|d\|_2 / \|r\|_2$ . For each scenario, we plot the quadratic  $n\Psi_T^{m_{2,\alpha}^{\text{id}}}$  and its constrained maximizer  $\alpha^* = \Pi_{[0,1]}(-B_n/A_n)$ . Figure 4 confirms the geometric setting: when the human displacement points in the same direction as the AI error, or is orthogonal to it, the optimizer collapses to the AI boundary and no complementarity is obtained. A corrective direction is not sufficient by itself: at  $\theta = \frac{3\pi}{4}$  with small  $q$ , the unconstrained maximizer lies beyond the feasible segment, so the constrained optimum is at the human boundary and remains non-complementary. Positive complementarity appears only when the human displacement is both corrective and sufficiently long, as in the  $\theta = \frac{3\pi}{4}$  and  $\theta = \pi$  cases with interior optima.

## 5.2 The $N = 3$ Case and Complementarity Invariance Under Changes of Protocol

We now study the first nontrivial case in which the same prediction-task HAI admits distinct protocols. Let  $T_L = ((12)3)$  and  $T_R = (1(23))$  be the two rooted planar binary trees in  $\mathcal{Y}_3$ , and decorate their leaves with the fixed ordered

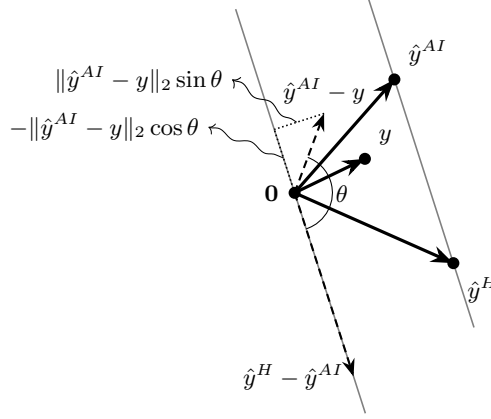


Figure 3: Geometry for the  $N = 2$  regression case with linear pooling. The segment of the line through  $\hat{y}^{AI}$  and  $\hat{y}^H$  that lies between the two vectors is the locus of feasible human–AI team predictions. The line through the origin  $\mathbf{0}$  is the human–AI disagreement direction. The vector  $\hat{y}^{AI} - y$  is projected onto this line and  $\theta$  is the angle between  $\hat{y}^{AI} - y$  and  $\hat{y}^H - \hat{y}^{AI}$ . The interior case inequalities (16) are both satisfied. Further, if  $\hat{y}^H - \hat{y}^{AI}$  is collinear with  $\hat{y}^{AI} - y$  but oppositely oriented, and if the projection of  $y$  lies inside the segment between  $\hat{y}^{AI}$  and  $\hat{y}^H$ , then  $\sin \theta = 0$  and the optimized value satisfies  $n\Psi_{\top}^{m_{2,\alpha}^{\text{id}},\alpha^*}(\hat{y}^H, \hat{y}^{AI}; D) = nK_n$ . Note that  $K_n$  is a function of  $\hat{y}^H$  and  $\hat{y}^{AI}$ —see (12).

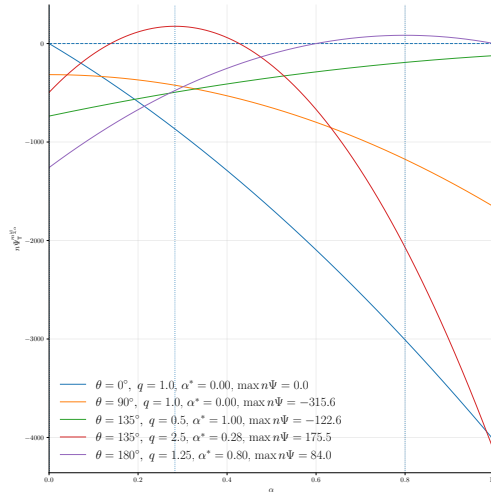


Figure 4:  $N = 2$  regression complementarity under linear pooling using the California housing dataset. Each curve shows the quadratic value of  $n\Psi_{\top}^{m_{2,\alpha}^{\text{id}},\alpha^*}$  [(\$100,000)<sup>2</sup>] as a function of the aggregation weight  $\alpha$ , for synthetic human predictions constructed by controlling the angle  $\theta$  between  $\hat{y}^H - \hat{y}^{AI}$  and  $\hat{y}^{AI} - y$ , and the relative displacement  $q = \|\hat{y}^H - \hat{y}^{AI}\|_2 / \|\hat{y}^{AI} - y\|_2$ . Vertical markers indicate the constrained optimizer.  $nK_n$  changes as a function of  $\hat{y}^H$ .

configuration (expert, assistant, AI) as in Figure 5. Thus,  $\top_L$  represents the protocol in which the expert and assistant first form an intermediate human judgment, which is then combined with the AI prediction. By contrast,  $\top_R$  represents the protocol in which the assistant first interacts with the AI, and the expert enters only at the final stage.

We compare the two protocols under local linear pooling. The same local parameters  $(\alpha_1, \alpha_2) \in [0, 1]^2$  are assigned according to the internal node ordering for each tree—see Figure 5. The corresponding outputs are

$$\hat{y}_{\top_L}(\alpha_1, \alpha_2) = \alpha_2(\alpha_1\hat{y}^{(1)} + (1 - \alpha_1)\hat{y}^{(2)}) + (1 - \alpha_2)\hat{y}^{(3)}, \quad (18)$$

and

$$\hat{y}_{\top_R}(\alpha_1, \alpha_2) = \alpha_1\hat{y}^{(1)} + (1 - \alpha_1)(\alpha_2\hat{y}^{(2)} + (1 - \alpha_2)\hat{y}^{(3)}). \quad (19)$$

Already at the symmetric value  $(\alpha_1, \alpha_2) = (\frac{1}{2}, \frac{1}{2})$ , the two protocols generally produce different outputs:

$$\hat{y}_{\mathbb{T}_L} = \frac{1}{4}\hat{y}^{(1)} + \frac{1}{4}\hat{y}^{(2)} + \frac{1}{2}\hat{y}^{(3)}, \quad \hat{y}_{\mathbb{T}_R} = \frac{1}{2}\hat{y}^{(1)} + \frac{1}{4}\hat{y}^{(2)} + \frac{1}{4}\hat{y}^{(3)}.$$

In  $\mathbb{T}_L$ , the AI receives the largest weight because it enters at the final composition step. In  $\mathbb{T}_R$ , the expert receives the largest weight instead. Hence, applying the same local averaging rule with the same local coordinates does not in general make the two protocols equivalent.

The question is therefore when the two protocols produce the same complementarity value. Under squared loss, Proposition 2 shows that this is a geometric equality condition: the two protocol outputs have the same complementarity value exactly when they are equally distant from the ground truth vector  $y$ . This motivates the following protocol-indifference locus.

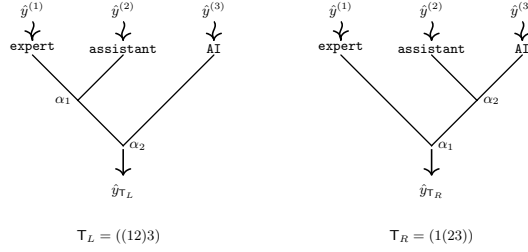


Figure 5: The two rooted planar binary trees for  $N=3$  and the ordered configuration (expert, assistant, AI), with corresponding prediction vectors  $\hat{y}^{(1)}$ ,  $\hat{y}^{(2)}$ , and  $\hat{y}^{(3)}$ . The trees represent two distinct protocols of the same prediction-task HAI:  $\mathbb{T}_L = ((12)3)$  first combines expert and assistant predictions, whereas  $\mathbb{T}_R = (1(23))$  first combines assistant and AI predictions. The vectors  $\hat{y}_{\mathbb{T}_L}$  and  $\hat{y}_{\mathbb{T}_R}$  denote the corresponding protocol outputs.

**Proposition 5** (Protocol-indifference locus for  $N=3$ ). *Let  $\mathbb{T}_L = ((12)3)$  and  $\mathbb{T}_R = (1(23))$  be the two  $N=3$  protocol trees above, equipped with local linear pooling and local parameters  $(\alpha_1, \alpha_2) \in [0, 1]^2$ . Define  $P_{\mathbb{T}_L, \mathbb{T}_R}(\alpha_1, \alpha_2)$  and the protocol-indifference locus  $\mathcal{S}_3$  as in Proposition 3. Then*

- (i)  $P_{\mathbb{T}_L, \mathbb{T}_R} = \sum_{0 \leq i, j \leq 2} A_{ij} \alpha_1^i \alpha_2^j$  has coefficients such that  $\sum_{0 \leq i, j \leq 2} A_{ij} = 0$ .
- (ii) If  $P_{\mathbb{T}_L, \mathbb{T}_R}(\alpha_1, \alpha_2) < 0$ , then  $\mathbb{T}_L$  has higher complementarity than  $\mathbb{T}_R$ . If  $P_{\mathbb{T}_L, \mathbb{T}_R}(\alpha_1, \alpha_2) > 0$ , then  $\mathbb{T}_R$  has higher complementarity than  $\mathbb{T}_L$ .
- (iii)  $(0, \alpha_2), (\alpha_1, 1) \in \mathcal{S}_3$ , where  $\alpha_1, \alpha_2 \in [0, 1]$ . At  $(0, 0)$ , both protocols collapse to the AI reliance; at  $(1, 1)$ , both collapse to expert reliance. In both cases, no complementarity is reached.

*Proof.* (i) For  $N=3$ , the recursive left-to-right ordering, the left tree keeps the parameter order  $(\alpha_1, \alpha_2)$ , while for the right tree  $\alpha_1$  is the root parameter and  $\alpha_2$  is the parameter of the internal node  $(23)$ . Writing  $\hat{y}_{\mathbb{T}_L}(\alpha_1, \alpha_2)$  as in (18) and  $\hat{y}_{\mathbb{T}_R}(\alpha_1, \alpha_2)$  as in (19) one obtains  $P_{\mathbb{T}_L, \mathbb{T}_R}(\alpha_1, \alpha_2) = \sum_{i, j=0}^2 A_{ij} \alpha_1^i \alpha_2^j$ , where the coefficients are

$$\begin{aligned} A_{00} &= A_{01} = A_{02} = 0, \\ A_{10} &= 2 \left\langle y - \hat{y}^{(3)}, \hat{y}^{(1)} - \hat{y}^{(3)} \right\rangle, \\ A_{20} &= - \left\| \hat{y}^{(1)} - \hat{y}^{(3)} \right\|_2^2, \\ A_{11} &= -2 \left( \left\langle y - \hat{y}^{(3)}, \hat{y}^{(1)} - \hat{y}^{(3)} \right\rangle + \left\langle \hat{y}^{(2)} - \hat{y}^{(3)}, \hat{y}^{(1)} - \hat{y}^{(3)} \right\rangle \right), \\ A_{12} &= A_{21} = 2 \left\langle \hat{y}^{(2)} - \hat{y}^{(3)}, \hat{y}^{(1)} - \hat{y}^{(3)} \right\rangle, \\ A_{22} &= \left\| \hat{y}^{(1)} - \hat{y}^{(3)} \right\|_2^2 - 2 \left\langle \hat{y}^{(2)} - \hat{y}^{(3)}, \hat{y}^{(1)} - \hat{y}^{(3)} \right\rangle. \end{aligned}$$

Finally,  $\sum_{0 \leq i, j \leq 2} A_{ij} = 0$  because  $\hat{y}_{\mathbb{T}_L}(1, 1) = \hat{y}_{\mathbb{T}_R}(1, 1) = \hat{y}^{(1)}$ . (ii) follows from the definition of  $P_{\mathbb{T}_L, \mathbb{T}_R}$  and (14). (iii) follows from  $\hat{y}_{\mathbb{T}_L}(\alpha_1, \alpha_2) - \hat{y}_{\mathbb{T}_R}(\alpha_1, \alpha_2) = \alpha_1(1 - \alpha_2)(\hat{y}^{(3)} - \hat{y}^{(1)})$ .  $\square$

### 5.2.1 Numerical illustration of the protocol-indifference locus for $N = 3$ regression.

We study when the two distinct  $N = 3$  trees  $T_L = ((12)3)$  and  $T_R = (1(23))$  induce the same complementarity value under linear local pooling by visualizing the protocol-indifference locus  $\mathcal{S}_3$  and studying the sign and zeros of  $P(\alpha_1, \alpha_2)$ , as characterized in Proposition 5. Using the held-out California Housing target vector and the same AI prediction vector as in the previous numerical illustration, we set  $\hat{y}^{(3)} = \hat{y}^{AI}$ , fix a corrective synthetic expert as  $\hat{y}^{(1)}$ , and vary the assistant prediction  $\hat{y}^{(2)}$  across four regimes: (i) weakly corrective; (ii) strongly corrective; (iii) weakly non-corrective; and (iv) strongly non-corrective. Here, ‘(non-)corrective’ refers to the displacement of the assistant prediction from the fixed AI prediction,  $\hat{y}^{(2)} - \hat{y}^{AI}$ , relative to the AI residual  $\hat{y}^{AI} - y$ : corrective displacements move against the AI residual, whereas non-corrective displacements reinforce it. All technical details are contained in Appendix F. Figure 6 shows the signed difference  $P(\alpha_1, \alpha_2)/n$  over the local-weight square. The thick black contour is  $\mathcal{S}_3$ , where both trees attain the same complementarity value. In regions where  $P(\alpha_1, \alpha_2) < 0$ ,  $T_L$  has the smaller squared loss and hence higher complementarity; in regions where  $P(\alpha_1, \alpha_2) > 0$ ,  $T_R$  has higher complementarity. Across the four regimes, the nontrivial branches of  $\mathcal{S}_3$  shift as the assistant displacement from the fixed AI prediction changes from corrective to non-corrective. Complementarity depends on tree topology: with the same ordered leaves and the same linear local rule, different protocol trees achieve higher complementarity in different regions of the weight space.

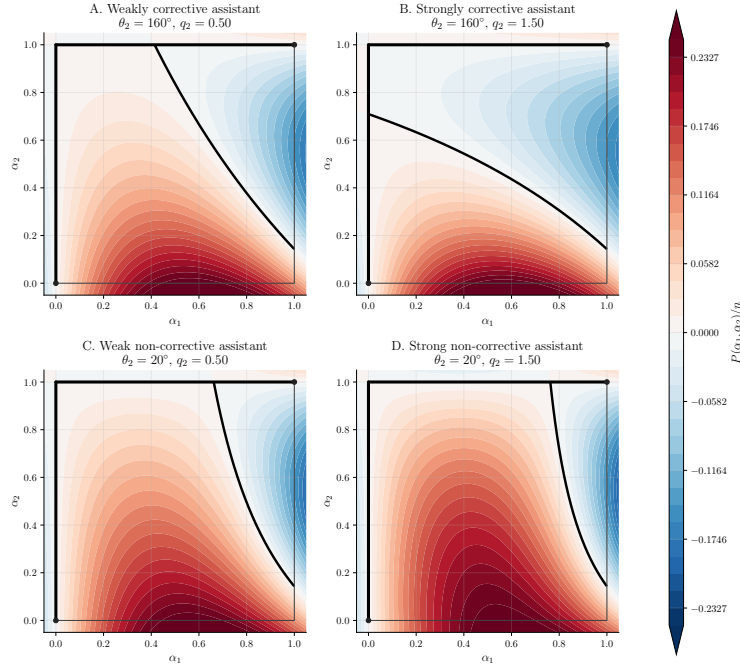


Figure 6:  $N = 3$  regression complementarity under linear pooling using the California housing dataset. Each panel shows the values of  $P(\alpha_1, \alpha_2)/n$  [(\$100,000)<sup>2</sup>] and the protocol-indifference locus  $P(\alpha_1, \alpha_2) = 0$  for the two protocol trees  $T_L = ((12)3)$  and  $T_R = (1(23))$ . Blue regions, where  $P(\alpha_1, \alpha_2) < 0$ , indicate higher complementarity for  $T_L$ ; red regions, where  $P(\alpha_1, \alpha_2) > 0$ , indicate higher complementarity for  $T_R$ , according to the sign convention in Proposition 5. The expert prediction  $\hat{y}^{(1)}$  is fixed with  $\theta_1 = 180^\circ$  and  $q_1 = 1.75$ , while the assistant prediction  $\hat{y}^{(2)}$  varies across four regimes. The protocol-indifference locus is shown only inside  $[0, 1]^2$ , boundaries included, by the thick black contour; it contains the branches  $\alpha_1 = 0$  and  $\alpha_2 = 1$ , while its interior branches depend on the assistant’s direction and magnitude relative to the AI residual.

### 5.3 The $N = 4$ Case and the (user, AI, AI, user) Agent Configuration

Finally, let us consider  $N = 4$  and the five rooted planar binary trees in  $Y_4$

$$T_1 = (((12)3)4), \quad T_2 = ((1(23))4), \quad T_3 = ((12)(34)), \quad T_4 = (1((23)4)), \quad T_5 = (1(2(34))).$$

We decorate their leaves with the ordered configuration (user, AI, AI, user). Here the two AI leaves may be interpreted as two copies or variants of the same AI system performing the same intended predictive function in possibly different deployment environments. We show these trees in Figure 7. They can be interpreted as follows.  $T_1$  is a *left-user*

*anchored sequential protocol*: the first user interacts with the first AI, then the second AI is added, and the second user enters only at the last stage. Tree  $T_2$  is an *AI-ensemble-first protocol with late human review*: the two AI systems are first pooled, then their output is combined with the first user, and finally with the second user.  $T_3$  represents *two parallel user-AI dyads*, whose outputs are then aggregated.  $T_4$  is again an *AI-ensemble-first protocol*, but with the order of the two users reversed. Finally,  $T_5$  is a *right-user anchored sequential protocol*. In real-world applications, certain protocols could be inaccessible due to constraints; however, this  $N = 4$  configuration example makes it possible to compare parallel human-AI dyads, AI-ensemble-first workflows, and serial protocols with late human intervention. In regression under squared loss and linear pooling, the  $N = 4$  case extends the  $N = 2$  and  $N = 3$  analyses in a direct way: each protocol tree induces a polynomial map from local weights  $(\alpha_1, \alpha_2, \alpha_3) \in [0, 1]^3$  to a global linear combination of the four leaf predictions, and complementarity is determined by the distance of that output from the ground-truth vector. We therefore do not introduce a separate numerical study for  $N = 4$ . Instead, we focus on the invariance of complementarity in regression under linear pooling as developed in the next sections.

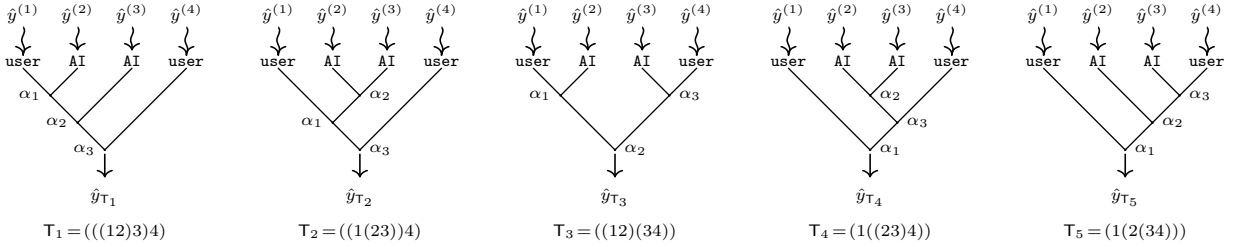


Figure 7: The five rooted planar binary trees for  $N = 4$  under the ordered configuration (user, AI, AI, user), with corresponding prediction vectors  $\hat{y}^{(1)}, \hat{y}^{(2)}, \hat{y}^{(3)}, \hat{y}^{(4)}$  and tree outputs  $\hat{y}_{T_1}, \dots, \hat{y}_{T_5}$ .

## 6 Trees in Regression Under Linear Pooling: Barycentric Coordinates

We turn now to the question whether in regression problems distinct protocols can lead to the same HAI output for the same parametrization of local interactions modeled by linear pooling, i.e.,  $m_{2,\alpha}^{\text{id}}(u, v) = \alpha u + (1 - \alpha)v$ . In this section, we show that, under linear local composition, every tree induces a convex combination of the leaf predictions. We make this global linear combination explicit through a barycentric coordinate map. To prove this, let us denote by  $\Delta^{N-1} := \{(\omega_1, \dots, \omega_N) \in [0, 1]^N : \sum_{j=1}^N \omega_j = 1\}$  the standard  $(N - 1)$ -simplex.

**Definition 6** (Barycentric coordinate map of a linear protocol tree). *Let  $T \in \mathcal{Y}_N$ . The barycentric coordinate map associated with  $T$  is the map  $\varphi_T : [0, 1]^{N-1} \rightarrow \Delta^{N-1}$ , defined recursively as follows. For the one-leaf tree  $|\in \mathcal{Y}_1$ , set  $\varphi_1(\emptyset) = (1) \in \Delta^0$ . For  $N \geq 2$ , let  $T = \sigma \vee \tau$ ,  $\sigma \in \mathcal{Y}_{N_1}$ ,  $\tau \in \mathcal{Y}_{N_2}$ ,  $N_1 + N_2 = N$ , be the unique root decomposition of  $T$ . With the recursive left-to-right order  $o(T) = \{\sigma < x < o(\tau)\}$  of internal nodes, for  $\alpha_{N-1}$ , the parameters  $(\alpha_1, \dots, \alpha_{N_1-1})$  belong to  $\sigma$ , the parameter  $\alpha_{N_1}$  belongs to the root, and the parameters  $(\alpha_{N_1+1}, \dots, \alpha_{N-1})$  belong to  $\tau$ . We define*

$$\varphi_T(\alpha) := \left( \alpha_{N_1} \varphi_\sigma(\alpha_1, \dots, \alpha_{N_1-1}), (1 - \alpha_{N_1}) \varphi_\tau(\alpha_{N_1+1}, \dots, \alpha_{N-1}) \right).$$

By construction, each component of  $\varphi_T(\alpha)$  lies in  $[0, 1]$ . Moreover, the components sum to one. Thus  $\varphi_T$  is well-defined as a map into  $\Delta^{N-1}$ . If  $\alpha \in (0, 1)^{N-1}$ , then all recursive scaling factors are strictly positive, and therefore  $\varphi_T(\alpha) \in \text{int}(\Delta^{N-1})$ .

The naming of  $\varphi_T$  follows from this observation: if the leaves of  $T$  are labeled by prediction vectors  $\hat{y}^{(1)}, \dots, \hat{y}^{(N)} \in \mathbb{R}^n$ , then the linear protocol output can be written as

$$\hat{y}_T(\alpha) = \sum_{j=1}^N \varphi_{T,j}(\alpha) \hat{y}^{(j)}, \quad \sum_{j=1}^N \varphi_{T,j}(\alpha) = 1. \quad (20)$$

This follows directly from the recursive definition of the linear pooling rule: the coefficients  $\varphi_{T,j}(\alpha)$  are the weights assigned by the tree to the  $j$ -th leaf prediction.

**Proposition 6.** *For every  $T \in \mathcal{Y}_N$ , the restriction*

$$\varphi_T|_{(0,1)^{N-1}} : (0, 1)^{N-1} \longrightarrow \text{int}(\Delta^{N-1})$$

*is a bijection.*

*Proof.* Appendix B. □

Proposition 6 shows that, once a protocol tree  $\mathbb{T}$  is fixed, its local linear-pooling parameters provide a coordinate system for the open simplex of leaf weights. Thus, *different local parameters of the same HAI protocol correspond to different barycentric weights assigned to the same ordered leaf predictions*. In the next section, we study whether different parameterizations of different trees can give rise to the *same* set of barycentric coordinates instead. The answer is positive and it provides an algebraic interpretation to complementarity invariance under tree reparameterization in regression.

## 7 Complementarity Invariance Across Trees in Regression: Tamari Covers and Reparameterizations

We study whether a change in tree topology can be absorbed by a corresponding change in local weights so that the two distinct trees produce the same root output and, therefore, the same complementarity level for any loss function. To answer this question we introduce the so-called Tamari moves on  $\mathcal{Y}_N$  [Tamari, 1962]. In HAI terms, a Tamari move changes the HAI protocol of a fixed ordered configuration by a local move that we describe in what follows.

**Definition 7** (Tamari cover, [Tamari, 1962]). *Let  $\mathbb{T}, \mathbb{T}' \in \mathcal{Y}_N$ . We say that  $\mathbb{T}'$  covers  $\mathbb{T}$  in the Tamari order, and write  $\mathbb{T} \prec_{\text{Tam}} \mathbb{T}'$ , if  $\mathbb{T}'$  is obtained from  $\mathbb{T}$  by a single right rotation, that is, by replacing a subtree of the form  $((AB)C)$  with  $(A(BC))$ , while preserving the left-to-right order of the leaves.*

The partial order generated by these cover relations is the *Tamari lattice* on  $\mathcal{Y}_N$ . Its Hasse diagram is the directed cover graph whose arrows are the Tamari covers. After forgetting orientations, this cover graph is the 1-skeleton of the associahedron  $\text{Assoc}_N$  [Stasheff, 1963], whose vertices are the trees in  $\mathcal{Y}_N$ .

**Definition 8** (Tamari reparameterization). *Let  $\mathbb{T}, \mathbb{T}' \in \mathcal{Y}_N$  satisfy  $\mathbb{T} \prec_{\text{Tam}} \mathbb{T}'$ . A Tamari reparameterization from  $\mathbb{T}$  to  $\mathbb{T}'$  is a map*

$$\Gamma_{\mathbb{T}, \mathbb{T}'} : (0, 1)^{N-1} \rightarrow (0, 1)^{N-1}$$

*such that, for every  $\alpha_{\mathbb{T}} \in (0, 1)^{N-1}$ , and every choice of leaf predictions  $\hat{y}^{(1)}, \dots, \hat{y}^{(N)}$ ,*

$$\hat{y}_{\mathbb{T}}(\alpha_{\mathbb{T}}) = \hat{y}_{\mathbb{T}'}(\Gamma_{\mathbb{T}, \mathbb{T}'}(\alpha_{\mathbb{T}})). \quad (21)$$

Thus, a Tamari reparameterization is a change of local coordinates along a Tamari cover that preserves the outputs of the trees of the cover. The restriction to the open cube excludes degenerate projection cases in which some internal weights are 0 or 1. Tamari reparameterizations are relevant in our setting as they preserve complementarity:

**Proposition 7.** *Assume regression with any loss. Let  $\mathbb{T}, \mathbb{T}' \in \mathcal{Y}_N$  satisfy  $\mathbb{T} \prec_{\text{Tam}} \mathbb{T}'$ , and let  $\Gamma_{\mathbb{T}, \mathbb{T}'} : (0, 1)^{N-1} \rightarrow (0, 1)^{N-1}$  be a Tamari reparameterization. Then, for all leaf predictions  $\hat{y}^{(1)}, \dots, \hat{y}^{(N)}$ , every dataset  $D$ , and  $\alpha_{\mathbb{T}} \in (0, 1)^{N-1}$ ,*

$$\Psi_{\mathbb{T}}^{m_{\mathbb{T}}(\alpha_{\mathbb{T}})}(\hat{y}^{(1)}, \dots, \hat{y}^{(N)}; D) = \Psi_{\mathbb{T}'}^{m_{\mathbb{T}'}(\Gamma_{\mathbb{T}, \mathbb{T}'}(\alpha_{\mathbb{T}}))}(\hat{y}^{(1)}, \dots, \hat{y}^{(N)}; D).$$

*Proof.* Equation (21) gives equality of the two root outputs after reparameterization. The claim follows from (7). □

Proposition 7 identifies a notion of *complementarity invariance along Hasse edges of the Tamari lattice*: distinct protocol trees related by a single Tamari cover may define the same value of the complementarity functional after an appropriate transport of local parameters for any choice of loss function of the regression problem, i.e., a Tamari reparameterization. We construct a Tamari reparameterization explicitly under local linear pooling:

**Theorem 2** (Existence of Tamari reparameterizations). *Assume regression with arbitrary pointwise loss and linear local composition  $m_{2, \beta}^{\text{id}}(u, v) = \beta u + (1 - \beta)v$ ,  $\beta \in (0, 1)$ . Let  $\mathbb{T} \in \mathcal{Y}_N$  contain a displayed subtree of the form  $((AB)C)$ , and let  $\mathbb{T}'$  be obtained from  $\mathbb{T}$  by the Tamari cover  $((AB)C) \mapsto (A(BC))$ . Then there exists a Tamari reparameterization*

$$\Gamma_{\mathbb{T}, \mathbb{T}'}^{\diamond} : (0, 1)^{N-1} \rightarrow (0, 1)^{N-1}.$$

*Consequently, for all leaf predictions  $\hat{y}^{(1)}, \dots, \hat{y}^{(N)}$ , every dataset  $D$ , and  $\alpha_{\mathbb{T}} \in (0, 1)^{N-1}$ ,*

$$\Psi_{\mathbb{T}}^{m_{\mathbb{T}}(\alpha_{\mathbb{T}})}(\hat{y}^{(1)}, \dots, \hat{y}^{(N)}; D) = \Psi_{\mathbb{T}'}^{m_{\mathbb{T}'}(\Gamma_{\mathbb{T}, \mathbb{T}'}^{\diamond}(\alpha_{\mathbb{T}}))}(\hat{y}^{(1)}, \dots, \hat{y}^{(N)}; D).$$

*Proof.* The construction is local. Let  $\gamma \in (0, 1)$  be the parameter at the root of  $AB$ , and let  $\delta \in (0, 1)$  be the parameter at the root of  $((AB)C)$ . All parameters outside the subtree  $((AB)C)$  are left unchanged by  $\Gamma_{\mathbb{T}, \mathbb{T}'}$ .

Define the two new parameters in the rotated fragment  $A(BC)$  by

$$\beta_{A(BC)} := \gamma\delta, \quad \beta_{BC} := \frac{\delta(1-\gamma)}{1-\gamma\delta}.$$

These parameters are again in  $(0, 1)$ :  $0 < \gamma\delta < 1$ , and  $1 - \gamma\delta > 0$ , while  $1 - \gamma\delta - \delta(1 - \gamma) = 1 - \delta > 0$ , so  $0 < \beta_{BC} < 1$ . Thus the construction defines a map  $\Gamma_{\mathbb{T}, \mathbb{T}'}^\diamond : (0, 1)^{N-1} \rightarrow (0, 1)^{N-1}$ . It remains to check that the displayed fragment has the same output before and after the transport  $\Gamma_{\mathbb{T}, \mathbb{T}'}^\diamond$ . Let  $z_A, z_B, z_C$  denote the outputs of the subtrees  $A, B, C$ . In  $\mathbb{T}$ , the fragment output is

$$\delta(\gamma z_A + (1 - \gamma)z_B) + (1 - \delta)z_C,$$

with coefficients  $\gamma\delta, \delta(1 - \gamma)$ , and  $1 - \delta$  on  $z_A, z_B, z_C$ . In  $\mathbb{T}'$ , the transported fragment output is

$$\beta_{A(BC)}z_A + (1 - \beta_{A(BC)})(\beta_{BC}z_B + (1 - \beta_{BC})z_C).$$

By the definitions above, the coefficient of  $z_A$  is  $\gamma\delta$ , the coefficient of  $z_B$  is  $(1 - \gamma\delta)\delta(1 - \gamma)/(1 - \gamma\delta) = \delta(1 - \gamma)$ , and the coefficient of  $z_C$  is  $1 - \delta$ . Hence the two fragment outputs are identical.

Since all parameters outside the fragment are unchanged, and since the rotated fragment supplies the same output to the rest of the tree, the full root outputs agree:  $\hat{y}_{\mathbb{T}}(\alpha_{\mathbb{T}}) = \hat{y}_{\mathbb{T}'}(\Gamma_{\mathbb{T}, \mathbb{T}'}^\diamond(\alpha_{\mathbb{T}}))$ . Then,  $\Gamma_{\mathbb{T}, \mathbb{T}'}^\diamond$  is a Tamari reparameterization by Definition 8. Applying Proposition 7 ends the proof.  $\square$

Theorem 2 gives complementarity invariance an algebraic and analytic form. The Tamari reparameterization result shows that, for any choice of the loss function and linear local composition, a Tamari cover determines an explicit transport of local parameters that preserves the entire protocol output. Thus *two protocol trees related by a Tamari move can be made analytically equivalent by a local change of coordinates on the interaction weights*.

For  $N = 3$ , the theorem immediately applies to the unique Tamari cover  $\mathbb{T}_L = ((12)3) \triangleleft_{\text{Tam}} \mathbb{T}_R = (1(23))$ . In HAI terms, the two workflows may have different procedures—expert–assistant aggregation followed by AI integration for  $\mathbb{T}_L$  versus assistant–AI aggregation followed by expert integration for  $\mathbb{T}_R$ —but, after the Tamari reparameterization  $\Gamma^\diamond$ , they induce the same root output and hence the same complementarity value.

For  $N = 4$ , Theorem 2 applies along cover relations in the five-tree Tamari lattice. Furthermore, for  $N = 4$ , we prove a coherence theorem: Tamari-cover reparameterizations satisfy the pentagon identity [Yanofsky, 2024]. We show this result graphically in Figure 8 and we state it more precisely in what follows:

**Theorem 3** (Tamari-cover reparameterizations satisfy the pentagon identity). *Assume regression with any loss and with linear local composition*

$$m_{2,\beta}^{\text{id}}(u, v) = \beta u + (1 - \beta)v, \quad \beta \in (0, 1).$$

Let  $\mathbb{T}_1 = (((12)3)4)$ ,  $\mathbb{T}_2 = ((1(23)4))$ ,  $\mathbb{T}_3 = ((12)(34))$ ,  $\mathbb{T}_4 = (1((23)4))$ ,  $\mathbb{T}_5 = (1(2(34)))$  be the five rooted planar binary trees in  $\mathcal{Y}_4$ , ordered by the Tamari covers. Let

$$\Gamma_{1,2}^\diamond, \Gamma_{1,3}^\diamond, \Gamma_{2,4}^\diamond, \Gamma_{3,5}^\diamond, \Gamma_{4,5}^\diamond$$

denote the Tamari-cover reparameterizations along the two directed paths from  $\mathbb{T}_1$  to  $\mathbb{T}_5$  as in Theorem 2. Then, for every parameter vector  $\alpha_{\mathbb{T}_1} \in (0, 1)^3$ , the pentagon identity holds:

$$(\Gamma_{3,5}^\diamond \circ \Gamma_{1,3}^\diamond)(\alpha_{\mathbb{T}_1}) = (\Gamma_{4,5}^\diamond \circ \Gamma_{2,4}^\diamond \circ \Gamma_{1,2}^\diamond)(\alpha_{\mathbb{T}_1}). \quad (22)$$

Consequently, for all leaf predictions  $\hat{y}^{(1)}, \dots, \hat{y}^{(4)}$ , every dataset  $D$ , and  $\alpha_{\mathbb{T}_1} \in (0, 1)^3$ ,

$$\begin{aligned} & \Psi_{\mathbb{T}_1}^{m_{\mathbb{T}_1}}(\alpha_{\mathbb{T}_1})(\hat{y}^{(1)}, \hat{y}^{(2)}, \hat{y}^{(3)}, \hat{y}^{(4)}; D) = \\ & \Psi_{\mathbb{T}_5}^{m_{\mathbb{T}_5}}(\Gamma_{3,5}^\diamond \circ \Gamma_{1,3}^\diamond(\alpha_{\mathbb{T}_1}))(\hat{y}^{(1)}, \hat{y}^{(2)}, \hat{y}^{(3)}, \hat{y}^{(4)}; D) = \\ & \Psi_{\mathbb{T}_5}^{m_{\mathbb{T}_5}}(\Gamma_{4,5}^\diamond \circ \Gamma_{2,4}^\diamond \circ \Gamma_{1,2}^\diamond(\alpha_{\mathbb{T}_1}))(\hat{y}^{(1)}, \hat{y}^{(2)}, \hat{y}^{(3)}, \hat{y}^{(4)}; D). \end{aligned} \quad (23)$$

*Proof.* Appendix C.  $\square$

Finally, we close the regression analysis by combining barycentric coordinates from Section 6 and Tamari reparameterizations described so far. Let  $\mathbb{T} \triangleleft_{\text{Tam}} \mathbb{T}'$  be a Tamari cover, with  $\mathbb{T}, \mathbb{T}' \in \mathcal{Y}_N$  and let  $\Gamma_{\mathbb{T}, \mathbb{T}'}^\diamond$  be the corresponding reparameterization from Theorem 2. Then Proposition 6 and Theorem 2 state that  $\varphi_{\mathbb{T}'} \circ \Gamma_{\mathbb{T}, \mathbb{T}'}^\diamond = \varphi_{\mathbb{T}}$  on  $(0, 1)^{N-1}$ . Equivalently, the following diagram commutes:

$$\begin{array}{ccc}
 (0, 1)^{N-1} & \xrightarrow{\Gamma_{\mathbb{T}, \mathbb{T}'}^\diamond} & (0, 1)^{N-1} \\
 \searrow \varphi_{\mathbb{T}} & & \swarrow \varphi_{\mathbb{T}'} \\
 & \text{int}(\Delta^{N-1}) & 
 \end{array}$$

Thus, the barycentric weights of a tree  $\mathbb{T} \in \mathcal{Y}_N$  are invariant under a Tamari cover of  $\mathbb{T}$  and a Tamari reparameterization of its parameters on  $(0, 1)^{N-1}$ .

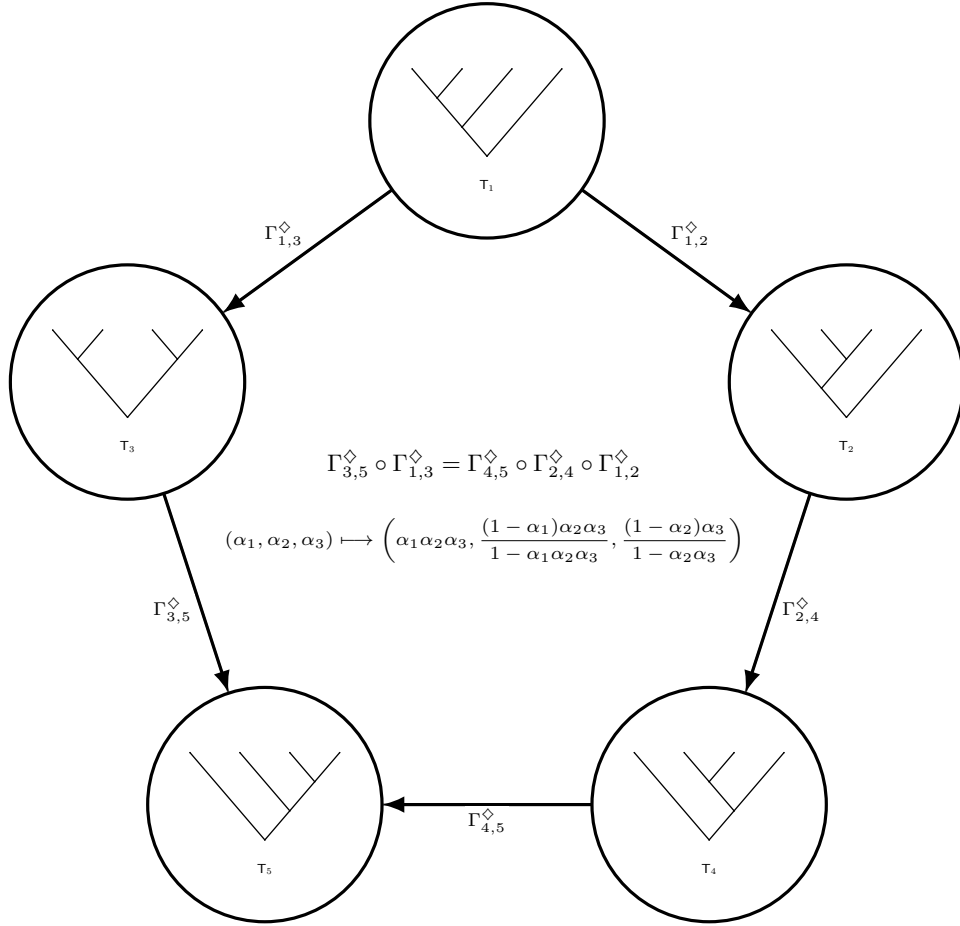


Figure 8: The pentagon identity satisfied by the Tamari-cover reparameterizations for  $N = 4$ . The vertices of the 1-skeleton of the associahedron  $\text{Assoc}_4$  are the five rooted planar binary trees in  $\mathcal{Y}_4$ . Edges represent Tamari cover moves. The two highlighted directed paths from the left comb  $\mathbb{T}_1$  to the right comb  $\mathbb{T}_5$  induce the same reparameterization. By Theorem 2, both paths preserve the root output and therefore the tree-relative complementarity functional.

## 8 Complementarity in Binary Classification

We now investigate complementarity in binary classification, with labels  $y_i \in \{0, 1\} = \mathcal{Y}$  and predicted probabilities  $\hat{y}_i \in (0, 1) = \hat{\mathcal{Y}}$ , where  $\hat{y}_i$  denotes the predicted probability of class 1.

**Definition 9** (Endpoint-monotone loss). *A loss function  $\ell : \mathcal{Y} \times \hat{\mathcal{Y}} \rightarrow [0, \infty)$  is called endpoint-monotone if  $\hat{y} \mapsto \ell(0, \hat{y})$  is nondecreasing and  $\hat{y} \mapsto \ell(1, \hat{y})$  is nonincreasing on  $(0, 1)$ .*

Thus, under endpoint-monotonicity, when the true label is 0, assigning more probability to class 1 cannot decrease the loss; when the true label is 1, assigning more probability to class 1 cannot increase the loss. This condition is satisfied by the main probabilistic classification losses used in practice.

**Proposition 8.** *The following binary classification losses are endpoint-monotone:*

- (i)  $\ell_F(y, \hat{y}) = D_F(y, \hat{y})$ , where  $D_F$  is a Bregman divergence generated by a convex  $F$  on  $[0, 1]$ , differentiable on  $(0, 1)$ , and with finite endpoint values [Bregman, 1967];
- (ii)  $\ell_f(y, \hat{y}) = D_f(P_y \| Q_{\hat{y}})$ , where  $D_f$  is an  $f$ -divergence between the Bernoulli distributions of ground truth and predicted probabilities, with  $f : [0, \infty) \rightarrow \mathbb{R}$  convex, finite on  $[0, \infty)$ , differentiable on  $(0, \infty)$ , and normalized by  $f(1) = 0$  [Ali and Silvey, 1966].

*Proof.* Appendix D. □

**Corollary 3.** *The following binary classification losses are endpoint-monotone: the Brier loss, binary cross-entropy/Kullback-Leibler loss, squared Hellinger loss, Pearson  $\chi^2$  loss, Jensen–Shannon loss, and Tsallis  $f$ -divergence losses [Tsallis, 1988, Furuichi et al., 2004].*

*Proof.* The Brier loss and binary cross-entropy are Bregman losses, generated respectively by  $F(\hat{y}) = \hat{y}^2$  and by the negative entropy  $F(\hat{y}) = \hat{y} \log \hat{y} + (1 - \hat{y}) \log(1 - \hat{y})$ . The remaining examples are  $f$ -divergence losses, with  $f : [0, \infty) \rightarrow \mathbb{R}$ . Squared Hellinger is generated, up to normalization, by  $f(t) = \frac{1}{2}(\sqrt{t} - 1)^2$ ; Pearson  $\chi^2$  by  $f(t) = (t - 1)^2$ ; Jensen–Shannon by

$$f(t) = \frac{1}{2} \left[ t \log \frac{2t}{1+t} + \log \frac{2}{1+t} \right];$$

and Tsallis  $f$ -divergences, for  $q > 0, q \neq 1$ , by the normalized generator  $f_q(t) = \frac{t^q - t}{q-1}$ . These generators are convex, differentiable on  $(0, \infty)$ , normalized by  $f(1) = 0$  and finite at 0. Proposition 8 therefore applies. □

## 8.1 An Impossibility Theorem for Complementarity in Binary Classification

We now obtain a structural impossibility result for binary classification. The result derives from combining endpoint-monotonicity of loss functions and a local condition on interaction rules in the trees.

**Definition 10** (Internality property of local rules). *A local rule  $m_2 : (0, 1)^n \times (0, 1)^n \rightarrow (0, 1)^n$  satisfies the internality property if, for every  $u, v \in (0, 1)^n$  and every coordinate  $i$ ,  $\min\{u_i, v_i\} \leq (m_2(u, v))_i \leq \max\{u_i, v_i\}$ .*

Internality captures interaction rules that interpolate between available predicted probabilities. This is a standard property of quasi-arithmetic means [Kolmogorov, 1930, Nagumo, 1930]:

**Lemma 2.** *Let  $m_2^p$  be a quasi-arithmetic mean. Then it satisfies the internality property.*

We begin with an observation: the internality property is preserved through tree composition.

**Lemma 3.** *Let  $m_2$  satisfy the internality property, let  $\mathsf{T} \in \mathsf{Y}_N$ , and fix a case  $i$ . If  $\hat{y}_i^{(1)}, \dots, \hat{y}_i^{(N)} \in (0, 1)$  are the leaf probabilities on that case and  $\hat{y}_i^{\mathsf{T}}$  is the output produced by  $\mathsf{T}$ , then*

$$\min_{1 \leq j \leq N} \hat{y}_i^{(j)} \leq \hat{y}_i^{\mathsf{T}} \leq \max_{1 \leq j \leq N} \hat{y}_i^{(j)}. \quad (24)$$

*Proof.* Proceed by induction on the number of leaves of  $\mathsf{T}$ . The case of one leaf is immediate. For the inductive step, suppose the root of  $\mathsf{T}$  combines two subtrees  $\mathsf{T}_L$  and  $\mathsf{T}_R$ , with outputs  $u_i$  and  $v_i$  on case  $i$ . By the inductive hypothesis, each of  $u_i$  and  $v_i$  lies in the interval spanned by the leaf probabilities  $\hat{y}_i^{(1)}, \dots, \hat{y}_i^{(N)}$ . Since  $m_2$  is internal,  $\hat{y}_i^{\mathsf{T}} = m_2(u_i, v_i)$  lies between  $u_i$  and  $v_i$ , hence also in the interval spanned by the leaves. □

Then we arrive at:

**Theorem 4** (Impossibility of complementarity in binary classification). *Let  $N \geq 2$ , let  $\mathsf{T} \in \mathsf{Y}_N$ , and let  $D = \{(x_i, y_i)\}_{i=1}^n$  be a labeled dataset with  $y_i \in \{0, 1\}$ . Let  $\hat{y}^{(1)}, \dots, \hat{y}^{(N)} \in (0, 1)^n$  be any collection of prediction vectors on  $D$ . If  $m_2$  satisfies the internality property, for every endpoint-monotone binary loss  $\ell$  in Definition 9,*

$$\Psi_{\mathsf{T}}^{m_2}(\hat{y}^{(1)}, \dots, \hat{y}^{(N)}; D) \leq 0.$$

*Proof.* By Lemma 3, for every case  $i$ ,  $\min_{1 \leq j \leq N} \hat{y}_i^{(j)} \leq \hat{y}_i^\top \leq \max_{1 \leq j \leq N} \hat{y}_i^{(j)}$ . If  $y_i = 0$ , endpoint monotonicity gives

$$\ell(0, \hat{y}_i^\top) \geq \ell\left(0, \min_{1 \leq j \leq N} \hat{y}_i^{(j)}\right) = \min_{1 \leq j \leq N} \ell(0, \hat{y}_i^{(j)}).$$

If  $y_i = 1$ , endpoint monotonicity gives

$$\ell(1, \hat{y}_i^\top) \geq \ell\left(1, \max_{1 \leq j \leq N} \hat{y}_i^{(j)}\right) = \min_{1 \leq j \leq N} \ell(1, \hat{y}_i^{(j)}).$$

Therefore, for every  $i = 1, \dots, n$ , we have that  $\min_{1 \leq j \leq N} \ell(y_i, \hat{y}_i^{(j)}) \leq \ell(y_i, \hat{y}_i^\top)$ . Averaging over  $i$  gives

$$\frac{1}{n} \sum_{i=1}^n \min_{1 \leq j \leq N} \ell(y_i, \hat{y}_i^{(j)}) \leq \frac{1}{n} \sum_{i=1}^n \ell(y_i, \hat{y}_i^\top).$$

Thus

$$\Psi_{\top}^{m\tau}(\hat{y}^{(1)}, \dots, \hat{y}^{(N)}; D) \leq 0. \quad \square$$

**Corollary 4.** *In binary classification, complementarity cannot be achieved by any internal local rule when the loss is one of the Bregman or finite Bernoulli  $f$ -divergence losses covered by Proposition 8.*

**Remark 2** (Multiclass cross-entropy). *The same obstruction holds in multiclass problems under cross-entropy. Let  $K \geq 2$ , let each agent output probabilities  $\hat{y}_i^{(j)} \in \text{int}(\Delta^{K-1})$ , and let  $\bar{k}(i)$  denote the true class of sample  $i$ . For multiclass cross-entropy,  $\ell(y_i, \hat{y}_i) = -\log \hat{y}_{i, \bar{k}(i)}$ , the tree-relative complementarity functional can be written as*

$$n\Psi_{\top}^{m\tau} = \sum_{i=1}^n \log \left( \frac{\hat{y}_{i, \bar{k}(i)}^\top}{\max_{1 \leq j \leq N} \hat{y}_{i, \bar{k}(i)}^{(j)}} \right).$$

Let  $m_2 : \text{int}(\Delta^{K-1}) \times \text{int}(\Delta^{K-1}) \rightarrow \text{int}(\Delta^{K-1})$  be a local rule. If  $m_2$  satisfies the internality property coordinatewise, i.e., for every class  $k$ ,  $(m_2(u, v))_k \in [\min\{u_k, v_k\}, \max\{u_k, v_k\}]$ , then  $\hat{y}_{i, \bar{k}(i)}^\top \leq \max_{1 \leq j \leq N} \hat{y}_{i, \bar{k}(i)}^{(j)}$  for every  $i$ , and hence  $\Psi_{\top}^{m\tau} \leq 0$ .

In summary, Theorem 4 identifies two sources of obstruction to complementarity in binary classification: endpoint-monotone losses combined with internal local rules cannot outperform the pointwise best available leaf prediction. Hence, achieving complementarity in binary classification requires relaxing at least one of these two conditions. Relaxing endpoint monotonicity seems to be conceptually unattractive, since it encodes a natural requirement of loss functions in binary classification. The alternative is therefore to relax internality. A possibility to do this is to amplify a quasi-arithmetic logit score before mapping it back to probability space. For instance, the amplified logit rule becomes

$$(m_{2, \alpha, \lambda}^{\text{logit}}(u, v))_i := \sigma\left(\lambda[\alpha \text{logit}(u_i) + (1 - \alpha) \text{logit}(v_i)]\right), \quad (25)$$

where  $\sigma(t) = (1 + e^{-t})^{-1}$ ,  $t \in \mathbb{R}$  and  $\lambda \geq 1$ . In HAI terms, amplification moves the combined prediction of two agents away from the zero in logit space, or equivalently away from probability  $\sigma(0) = \frac{1}{2}$ , in the direction selected by the agents' pooled log-odds predictions. Note that the rule  $m_{2, \alpha, \lambda}^{\text{logit}}$  is normalized logarithmic pooling of Bernoulli forecasts [Neyman and Roughgarden, 2023a,b] if  $\lambda = 1$ . For  $N = 2$ , the effect of amplifying the logit rule on complementarity is explicitly derived. Write

$$z_i(\alpha) := \alpha \text{logit}(\hat{y}_i^{(1)}) + (1 - \alpha) \text{logit}(\hat{y}_i^{(2)}), \quad m_i^{\alpha, \lambda} := \sigma(\lambda z_i(\alpha)).$$

Under binary cross-entropy, with  $I_1 = \{i : y_i = 1\}$  and  $I_0 = \{i : y_i = 0\}$ , the amplified logit rule gives the complementarity functional

$$n\Psi^{\alpha, \lambda} = \sum_{i \in I_1} \left[ -\log \max\{\hat{y}_i^{(1)}, \hat{y}_i^{(2)}\} - \log(1 + e^{-\lambda z_i(\alpha)}) \right] + \sum_{i \in I_0} \left[ -\log \max\{1 - \hat{y}_i^{(1)}, 1 - \hat{y}_i^{(2)}\} - \log(1 + e^{\lambda z_i(\alpha)}) \right].$$

Thus, for  $i \in I_1$ , the  $i$ -th summand is positive if and only if  $(m_{2, \alpha, \lambda}^{\text{logit}}(\hat{y}^{(1)}, \hat{y}^{(2)}))_i > \max\{\hat{y}_i^{(1)}, \hat{y}_i^{(2)}\}$ . For  $i \in I_0$ , it is positive if and only if  $(m_{2, \alpha, \lambda}^{\text{logit}}(\hat{y}^{(1)}, \hat{y}^{(2)}))_i < \min\{\hat{y}_i^{(1)}, \hat{y}_i^{(2)}\}$ . For these local complementarity cases the non-internal output  $m_{2, \alpha, \lambda}^{\text{logit}}(\hat{y}^{(1)}, \hat{y}^{(2)})$  must move outside the interval spanned by the two input probabilities, and it must do so in the direction of the true class. We analyze this point empirically in the section that follows.

### 8.1.1 Numerical illustration of complementarity for binary classification beyond internality

We study complementarity in the  $N = 2$  binary-classification case under cross-entropy using synthetic pairs of probabilistic predictors. We fix  $\alpha = 0.5$  and evaluate the amplified logit rule from Equation (25) for several amplification levels  $\lambda \geq 1$ . For each simulated pair, we compute the global complementarity value  $n\Psi$  and the class-wise rates  $k_0$  and  $k_1$  of canonical local complementarity: on  $I_0$ , the pooled prediction lies below both input probabilities, while on  $I_1$ , it lies above both input probabilities. At  $\lambda = 1$ , ordinary internal logit pooling cannot satisfy these strict outside-interval conditions, in line with Theorem 4. For  $\lambda > 1$ , amplification can generate such local complementarity cases by moving the pooled logit away from 0, toward class 0 or class 1 depending on its sign. Figure 9 shows that larger values of  $k_0$  and  $k_1$  are associated with positive global complementarity, although the relation is not deterministic: because cross-entropy is unbounded, a small number of amplified wrong-sign cases can outweigh many locally positive gains.

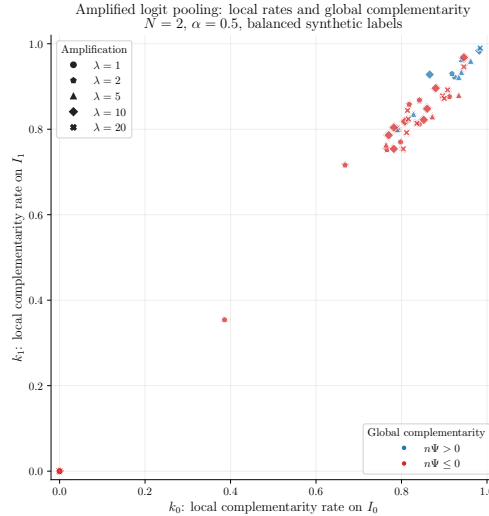


Figure 9:  $N = 2$  binary classification under cross-entropy with amplified logit pooling and fixed  $\alpha = 0.5$ . Each point is one simulated pair of probabilistic predictors, plotted by the class-wise rates  $(k_0, k_1)$  of canonical local complementarity: for  $y_i = 0$ , the pooled prediction lies below both input probabilities; for  $y_i = 1$ , it lies above both input probabilities.

Color indicates global complementarity: blue points satisfy  $n\Psi_{\text{T}}^{\text{logit}, m_{2, \alpha, \lambda}} > 0$ , while red points do not. The plot illustrates that larger local-complementarity rates are associated with positive global complementarity, although the relation is not deterministic because cross-entropy losses can be dominated by a small number of amplified wrong-sign cases.

## 9 Discussion and Conclusions

We provided a tree-based mathematical language for formalizing complementarity as a property of HAI protocols. We summarize the implications for HAI of our formalism in four messages.

First, *complementarity is not reliance*. If an HAI protocol only selects among existing agent predictions, as in self-reliance or AI-reliance, then it cannot achieve complementarity relative to the pointwise-min oracle benchmark. This holds regardless of task, loss, or prediction quality. Appropriate reliance may still be valuable in certain real-world HAI settings [Schemmer et al., 2023], but it is not sufficient for complementarity in the strict sense studied here. In summary, complementarity requires aggregation of input predictions beyond choosing one among them.

Second, *in two-agent regression under squared loss, human-AI complementarity is about AI residual correction*. In this setting, maximizing complementarity is equivalent to moving the human-AI interaction protocol output closer to the ground-truth vector. In the linear aggregation case, the optimal weight is determined by the projection of the ground truth onto the line segment between the two predictions. Thus, complementarity depends on whether the human-AI disagreement direction corrects the AI residual, and whether the correction is large enough to place the projection of ground truth inside the feasible pooling segment. This gives a geometric interpretation of why some human-AI disagreements in real-world HAIs may be useful and others are not.

Third, *in regression, HAI protocol matters when formalizing complementarity, but complementarity invariance across protocol trees is possible*. For  $N \geq 3$ , non-associative local aggregation makes the protocol tree a design variable:

the same ordered agents and the same local rule can lead to different outputs and different complementarity values. The  $N = 3$  protocol-indifference analysis shows that the equality locus contains boundary components induced by degenerate local weights and nontrivial interior branches determined by the geometry of the prediction vectors. At the same time, the dependence of HAI protocols on tree topology does not mean that every protocol tree change is substantively different. The barycentric and Tamari results show that some protocol changes can be compensated by an appropriate transport of local parameters. Under linear pooling, trees provide different coordinate charts for the same simplex of leaf weights, and Tamari-cover reparameterizations preserve complementarity by preserving the induced barycentric output. For  $N = 4$ , the two directed Tamari paths from the left comb to the right comb induce the same reparameterization. This shows that the invariance satisfies the pentagon identity.

Lastly, in *binary classification under standard loss functions, interpolation of agent predictions is insufficient to reach complementarity*. This obstruction holds for endpoint-monotone losses, including cross-entropy and standard Bregman or many finite Bernoulli  $f$ -divergence losses, whenever the local aggregation rule satisfies the internality property. In particular, quasi-arithmetic means fall under the impossibility theorem. Although amplified logit pooling can help escape the impossibility theorem, as shown in the numerical simulation in Section 8.1.1, the classification impossibility theorem is a negative result for HAI research. Thus, if one accepts the pointwise-min oracle benchmark as the relevant standard for complementarity in certain high-stakes HAI domains, then many common human–AI classification protocols cannot achieve complementarity by interpolating between human and AI probabilities [Vaccaro et al., 2024]. This matters for the HAI research domain and calls for a revision of the empirical approach to complementarity in classification tasks.

Future work can extend the proposed framework in different directions. These include adding explicit costs for interaction depth, monitoring burden, and protocol complexity—see *efficient complementarity* in [Ferrario et al., 2026]—in the optimization problems (9) and (10); integrating feasibility constraints arising from fairness, robustness, oversight, documentation, and domain-specific workflow rules within trees; studying the stability of complementarity under dataset shift and temporal change; and testing the framework on real human–AI and multi-agent prediction settings.

## Acknowledgments

This work was partly conducted within the framework of the EUonAIR Centre of Excellence in Responsible AI and Education. It was partially supported by a grant from Movetia, funded by the Swiss Confederation. We also thank Alessandro Facchini and Matteo Casserini for many useful conversations on complementarity and human–AI interactions.

## Appendix

### A Proof of Proposition 4

*Proof.* Write

$$\sum_{i=1}^n (\alpha \hat{y}_i^H + (1 - \alpha) \hat{y}_i^{AI} - y_i)^2 = A_n \alpha^2 + 2B_n \alpha + C_n,$$

where

$$A_n = \|\hat{y}^H - \hat{y}^{AI}\|_2^2, \quad B_n = \langle \hat{y}^H - \hat{y}^{AI}, \hat{y}^{AI} - y \rangle, \quad C_n = \|\hat{y}^{AI} - y\|_2^2.$$

Thus

$$n\Psi_{\mathcal{T}}^{m_{2,\alpha}^{\text{id}}} = -A_n \alpha^2 - 2B_n \alpha + (nK_n - C_n),$$

which is Equation (15), where

$$nK_n = \sum_{i=1}^n \min\{(y_i - \hat{y}_i^H)^2, (y_i - \hat{y}_i^{AI})^2\}.$$

If  $A_n = 0$ , then  $\hat{y}^H = \hat{y}^{AI}$ , hence  $B_n = 0$ ,  $nK_n = C_n$ , and  $n\Psi_{\mathcal{T}}^{m_{2,\alpha}^{\text{id}}} = 0$  for all  $\alpha \in [0, 1]$ . Thus every  $\alpha \in [0, 1]$  is optimal, but no complementarity is possible.

Assume now that  $A_n > 0$ . The function

$$Q(\alpha) := -A_n \alpha^2 - 2B_n \alpha + (nK_n - C_n)$$

is a strictly concave quadratic on  $[0, 1]$ . Its derivative is  $Q'(\alpha) = -2A_n\alpha - 2B_n$ , so the unconstrained maximizer is  $\alpha_0 = -\frac{B_n}{A_n}$ . Restricting to  $[0, 1]$  gives the unique constrained maximizer  $\alpha^* = \Pi_{[0,1]}\left(-\frac{B_n}{A_n}\right)$ . Equivalently,

$$\alpha^* = \begin{cases} 0, & B_n \geq 0, \\ -\frac{B_n}{A_n}, & -A_n < B_n < 0, \\ 1, & B_n \leq -A_n. \end{cases}$$

The optimized value is

$$n\Psi_{\mathbb{T}}^{m_{2,\alpha^*}^{\text{id}}} = nK_n - (A_n(\alpha^*)^2 + 2B_n\alpha^* + C_n).$$

In the interior case  $-A_n < B_n < 0$ , this becomes

$$n\Psi_{\mathbb{T}}^{m_{2,\alpha^*}^{\text{id}}} = nK_n - C_n + \frac{B_n^2}{A_n}.$$

Equivalently, the optimized squared loss of the aggregate is

$$C_n - \frac{B_n^2}{A_n}.$$

At the endpoints, the aggregate reduces to one of the standalone predictions:

$$\alpha^* = 0 \quad \Rightarrow \quad n\Psi_{\mathbb{T}}^{m_{2,0}^{\text{id}}} = nK_n - \|\hat{y}^{AI} - y\|_2^2 \leq 0,$$

and

$$\alpha^* = 1 \quad \Rightarrow \quad n\Psi_{\mathbb{T}}^{m_{2,1}^{\text{id}}} = nK_n - \|\hat{y}^H - y\|_2^2 \leq 0.$$

Therefore complementarity, when it occurs, can only occur in the interior case.  $\square$

## B Proof of Proposition 6

*Proof.* We prove that, for every  $\mathbb{T} \in \mathcal{Y}_N$ , the restriction  $\varphi_{\mathbb{T}}|_{(0,1)^{N-1}} : (0,1)^{N-1} \rightarrow \text{int}(\Delta^{N-1})$  is a bijection.

Let

$$\mathbb{T} = \sigma \vee \tau \in \mathcal{Y}_N, \quad \sigma \in \mathcal{Y}_{N_1}, \quad \tau \in \mathcal{Y}_{N_2}, \quad N_1 + N_2 = N.$$

With respect to the recursive left-to-right ordering of internal nodes, the root of  $\mathbb{T}$  has index  $N_1$ . Hence every parameter vector  $\alpha \in (0,1)^{N-1}$  decomposes as  $\alpha = (\alpha_L, \alpha_{N_1}, \alpha_R)$ , where  $\alpha_L = (\alpha_1, \dots, \alpha_{N_1-1})$ ,  $\alpha_R = (\alpha_{N_1+1}, \dots, \alpha_{N-1})$ . By definition,

$$\varphi_{\mathbb{T}}(\alpha) = (\alpha_{N_1}\varphi_{\sigma}(\alpha_L), (1 - \alpha_{N_1})\varphi_{\tau}(\alpha_R)).$$

Injectivity of  $\varphi_{\mathbb{T}}$  is equivalent to

$$\varphi_{\mathbb{T}}(\alpha) = \varphi_{\mathbb{T}}(\beta) \quad \Longrightarrow \quad \alpha = \beta. \quad (26)$$

We prove this by induction on  $N$ . For  $N = 1$ , the claim is trivial, since  $\varphi(|; \emptyset) = (1)$ . For  $N = 2$ , the unique tree satisfies  $\varphi_{\mathbb{T}}(\alpha) = (\alpha, 1 - \alpha)$ , so (26) holds. Assume injectivity holds for all trees with fewer than  $N$  leaves, and let  $\mathbb{T} = \sigma \vee \tau \in \mathcal{Y}_N$ . Let

$$\alpha = (\alpha_L, \alpha_{N_1}, \alpha_R), \quad \beta = (\beta_L, \beta_{N_1}, \beta_R),$$

and suppose  $\varphi_{\mathbb{T}}(\alpha) = \varphi_{\mathbb{T}}(\beta)$ . Equating the first  $N_1$  components and the last  $N_2$  components gives

$$\begin{aligned} \alpha_{N_1}\varphi_{\sigma,i}(\alpha_L) &= \beta_{N_1}\varphi_{\sigma,i}(\beta_L), & i &= 1, \dots, N_1, \\ (1 - \alpha_{N_1})\varphi_{\tau,j}(\alpha_R) &= (1 - \beta_{N_1})\varphi_{\tau,j}(\beta_R), & j &= 1, \dots, N_2. \end{aligned}$$

Summing the first line over  $i = 1, \dots, N_1$  and using  $\sum_i \varphi_{\sigma,i} = 1$  gives  $\alpha_{N_1} = \beta_{N_1}$ . Since  $\alpha_{N_1} \in (0, 1)$ , the first line then reduces to  $\varphi_{\sigma}(\alpha_L) = \varphi_{\sigma}(\beta_L)$ . By the induction hypothesis applied to  $\sigma$ , we obtain  $\alpha_L = \beta_L$ . Similarly,  $1 - \alpha_{N_1} = 1 - \beta_{N_1} > 0$ , so the second line reduces to  $\varphi_{\tau}(\alpha_R) = \varphi_{\tau}(\beta_R)$ . By the induction hypothesis applied to  $\tau$ , we obtain  $\alpha_R = \beta_R$ . Hence  $\alpha = \beta$ , proving injectivity.

Surjectivity of  $\varphi_{\mathbb{T}}$  is equivalent to

$$\forall \omega \in \text{int}(\Delta^{N-1}), \quad \exists \alpha \in (0,1)^{N-1} \quad \text{such that} \quad \varphi_{\mathbb{T}}(\alpha) = \omega. \quad (27)$$

We again argue by induction on  $N$ . For  $N = 1$ , the statement is trivial. For  $N = 2$ , it follows from  $\varphi_{\mathbb{T}}(\alpha) = (\alpha, 1 - \alpha)$ . Assume surjectivity holds for all trees with fewer than  $N$  leaves, and let  $\mathbb{T} = \sigma \vee \tau \in \mathbb{Y}_N$ . Then (27) is equivalent to

$$\begin{aligned}\omega_i &= \alpha_{N_1} \varphi_{\sigma,i}(\alpha_L), & i &= 1, \dots, N_1 \\ \omega_{N_1+j} &= (1 - \alpha_{N_1}) \varphi_{\tau,j}(\alpha_R), & j &= 1, \dots, N_2\end{aligned}$$

Summing over  $i = 1, \dots, N_1$  and  $j = 1, \dots, N_2$  gives

$$\alpha_{N_1} = \sum_{i=1}^{N_1} \omega_i, \quad 1 - \alpha_{N_1} = \sum_{j=1}^{N_2} \omega_{N_1+j}.$$

Then

$$\begin{aligned}\varphi_{\sigma,i}(\alpha_L) &= \frac{\omega_i}{\sum_{l=1}^{N_1} \omega_l}, & i &= 1, \dots, N_1 \\ \varphi_{\tau,j}(\alpha_R) &= \frac{\omega_{N_1+j}}{\sum_{s=1}^{N_2} \omega_{N_1+s}}, & j &= 1, \dots, N_2.\end{aligned}$$

The induction step gives  $\alpha_L$  and  $\alpha_R$ . This concludes the proof.  $\square$

## C The Pentagon Identity on the $N = 4$ Associahedron

*Proof.* To prove Theorem 3, we use the five trees  $\mathbb{T}_1 = (((12)3)4)$ ,  $\mathbb{T}_2 = ((1(23))4)$ ,  $\mathbb{T}_3 = ((12)(34))$ ,  $\mathbb{T}_4 = (1((23)4))$ ,  $\mathbb{T}_5 = (1(2(34)))$ , which form the vertices of the Stasheff associahedron  $\text{Assoc}_4$ ; see Figure 8. Throughout, we write  $\alpha = (\alpha_1, \alpha_2, \alpha_3) \in (0, 1)^3$  for the parameterization of the ‘left comb’  $\mathbb{T}_1$ , where  $\alpha_1$  labels the node  $(12)$ ,  $\alpha_2$  labels the node  $((12)3)$ , and  $\alpha_3$  labels the root.

### C.1 Path I: $\mathbb{T}_1 \rightarrow \mathbb{T}_3 \rightarrow \mathbb{T}_5$

First consider the cover

$$\mathbb{T}_1 = (((12)3)4) \longrightarrow \mathbb{T}_3 = ((12)(34)).$$

This rotates the fragment  $((AB)C)$  with

$$A = (12), \quad B = 3, \quad C = 4.$$

Hence, using the definition of the map  $\Gamma^\diamond$ , the parameters on  $\mathbb{T}_3$  are

$$\Gamma_{1,3}^\diamond(\alpha_1, \alpha_2, \alpha_3) = \left( \alpha_1, \alpha_2 \alpha_3, \frac{(1 - \alpha_2) \alpha_3}{1 - \alpha_2 \alpha_3} \right).$$

Here the coordinates on  $\mathbb{T}_3$  are ordered as: parameter at  $(12)$ , parameter at the root  $((12)(34))$ , and parameter at  $(34)$ . Next consider the cover

$$\mathbb{T}_3 = ((12)(34)) \longrightarrow \mathbb{T}_5 = (1(2(34))).$$

This rotates the root fragment

$$((AB)C) \longrightarrow (A(BC))$$

with

$$A = 1, \quad B = 2, \quad C = (34).$$

If we write

$$(\gamma_1, \gamma_2, \gamma_3) = \Gamma_{1,3}^\diamond(\alpha_1, \alpha_2, \alpha_3),$$

then

$$\Gamma_{3,5}^\diamond(\gamma_1, \gamma_2, \gamma_3) = \left( \gamma_1 \gamma_2, \frac{(1 - \gamma_1) \gamma_2}{1 - \gamma_1 \gamma_2}, \gamma_3 \right).$$

Substituting the values of  $\gamma_1, \gamma_2, \gamma_3$  gives

$$(\Gamma_{3,5}^\diamond \circ \Gamma_{1,3}^\diamond)(\alpha_1, \alpha_2, \alpha_3) = \left( \alpha_1 \alpha_2 \alpha_3, \frac{(1 - \alpha_1) \alpha_2 \alpha_3}{1 - \alpha_1 \alpha_2 \alpha_3}, \frac{(1 - \alpha_2) \alpha_3}{1 - \alpha_2 \alpha_3} \right). \quad (28)$$

## C.2 Path II: $\mathbb{T}_1 \rightarrow \mathbb{T}_2 \rightarrow \mathbb{T}_4 \rightarrow \mathbb{T}_5$

Now consider the cover

$$\mathbb{T}_1 = (((12)3)4) \longrightarrow \mathbb{T}_2 = ((1(23))4).$$

This rotates the fragment

$$((12)3) \longrightarrow (1(23)),$$

so  $A = 1, B = 2, C = 3$ . Therefore

$$\Gamma_{1,2}^\diamond(\alpha_1, \alpha_2, \alpha_3) = \left( \alpha_1 \alpha_2, \frac{(1 - \alpha_1) \alpha_2}{1 - \alpha_1 \alpha_2}, \alpha_3 \right).$$

Here the coordinates on  $\mathbb{T}_2$  are ordered as: parameter at  $(1(23))$ , parameter  $(23)$ , and parameter at the root. Next consider the cover

$$\mathbb{T}_2 = ((1(23))4) \longrightarrow \mathbb{T}_4 = (1((23)4)).$$

This rotates the root fragment with

$$A = 1, \quad B = (23), \quad C = 4.$$

If

$$(\delta_1, \delta_2, \delta_3) = \Gamma_{1,2}^\diamond(\alpha_1, \alpha_2, \alpha_3),$$

then

$$\Gamma_{2,4}^\diamond(\delta_1, \delta_2, \delta_3) = \left( \delta_1 \delta_3, \delta_2, \frac{(1 - \delta_1) \delta_3}{1 - \delta_1 \delta_3} \right).$$

Substituting gives

$$(\eta_1, \eta_2, \eta_3) := (\Gamma_{2,4}^\diamond \circ \Gamma_{1,2}^\diamond)(\alpha_1, \alpha_2, \alpha_3) = \left( \alpha_1 \alpha_2 \alpha_3, \frac{(1 - \alpha_1) \alpha_2}{1 - \alpha_1 \alpha_2}, \frac{(1 - \alpha_1 \alpha_2) \alpha_3}{1 - \alpha_1 \alpha_2 \alpha_3} \right). \quad (29)$$

Finally, consider the cover

$$\mathbb{T}_4 = (1((23)4)) \longrightarrow \mathbb{T}_5 = (1(2(34))).$$

This rotates the fragment

$$((23)4) \longrightarrow (2(34)),$$

so  $A = 2, B = 3, C = 4$ . Therefore

$$\Gamma_{4,5}^\diamond(\eta_1, \eta_2, \eta_3) = \left( \eta_1, \eta_2 \eta_3, \frac{(1 - \eta_2) \eta_3}{1 - \eta_2 \eta_3} \right).$$

Then, it follows that

$$\begin{aligned} 1 - \eta_2 &= \frac{(1 - \alpha_2)}{1 - \alpha_1 \alpha_2}, \\ \eta_2 \eta_3 &= \frac{(1 - \alpha_1) \alpha_2 \alpha_3}{1 - \alpha_1 \alpha_2 \alpha_3}, \\ 1 - \eta_2 \eta_3 &= \frac{1 - \alpha_2 \alpha_3}{1 - \alpha_1 \alpha_2 \alpha_3}, \\ \frac{(1 - \eta_2) \eta_3}{1 - \eta_2 \eta_3} &= \frac{(1 - \alpha_2) \alpha_3}{1 - \alpha_2 \alpha_3}. \end{aligned}$$

Collecting terms,

$$(\Gamma_{4,5}^\diamond \circ \Gamma_{2,4}^\diamond \circ \Gamma_{1,2}^\diamond)(\alpha_1, \alpha_2, \alpha_3) = \left( \alpha_1 \alpha_2 \alpha_3, \frac{(1 - \alpha_1) \alpha_2 \alpha_3}{1 - \alpha_1 \alpha_2 \alpha_3}, \frac{(1 - \alpha_2) \alpha_3}{1 - \alpha_2 \alpha_3} \right). \quad (30)$$

Comparing (28) and (30) proves

$$(\Gamma_{3,5}^\diamond \circ \Gamma_{1,3}^\diamond)(\alpha_1, \alpha_2, \alpha_3) = (\Gamma_{4,5}^\diamond \circ \Gamma_{2,4}^\diamond \circ \Gamma_{1,2}^\diamond)(\alpha_1, \alpha_2, \alpha_3),$$

which is Equation (22). This establishes the commutativity of the  $N = 4$  Stasheff pentagon at the level of reparameterizations. By Theorem 2, every edgewise transport preserves the root output. Hence both pathwise compositions preserve the root output from  $\mathbb{T}_1$  to  $\mathbb{T}_5$ , and therefore

$$\hat{y}_{\mathbb{T}_1}(\boldsymbol{\alpha}) = \hat{y}_{\mathbb{T}_5}((\Gamma_{3,5}^\diamond \circ \Gamma_{1,3}^\diamond)(\boldsymbol{\alpha})) = \hat{y}_{\mathbb{T}_5}((\Gamma_{4,5}^\diamond \circ \Gamma_{2,4}^\diamond \circ \Gamma_{1,2}^\diamond)(\boldsymbol{\alpha})).$$

Regression complementarity invariance then follows from Equation (7), proving Theorem 3.  $\square$

## D Proof of Proposition 8

*Proof.* For the Bregman case, let  $F : [0, 1] \rightarrow \mathbb{R}$  be convex and continuous on  $[0, 1]$ , and differentiable on  $(0, 1)$ . For  $y \in \{0, 1\}$  and  $\hat{y} \in (0, 1)$ , define  $D_F(y, \hat{y}) := F(y) - F(\hat{y}) - F'(\hat{y})(y - \hat{y})$ . We show endpoint monotonicity. Write  $\ell_F(0, \hat{y}) = F(0) - G_0(\hat{y})$  and  $\ell_F(1, \hat{y}) = F(1) - G_1(\hat{y})$ , where  $G_0(\hat{y}) := F(\hat{y}) - \hat{y}F'(\hat{y})$  and  $G_1(\hat{y}) := F(\hat{y}) + (1 - \hat{y})F'(\hat{y})$ . By convexity of  $F$ ,  $G_0$  is nonincreasing and  $G_1$  is nondecreasing on  $(0, 1)$ . Thus  $\ell_F = D_F$  is endpoint-monotone.

We now consider  $f$ -divergences. Under the standard convention

$$D_f(P\|Q) := \sum_{k \in \{0,1\}} Q_k f\left(\frac{P_k}{Q_k}\right),$$

let  $f : [0, \infty) \rightarrow \mathbb{R}$  be convex, differentiable on  $(0, \infty)$ , normalized by  $f(1) = 0$ , and finite at 0. For binary classification, write the hard-label distribution and the predicted distribution as  $P_y = (y, 1 - y)$  and  $Q_{\hat{y}} = (\hat{y}, 1 - \hat{y})$ . The induced hard-label loss is

$$\ell_f(y, \hat{y}) := D_f(P_y\|Q_{\hat{y}}) = \hat{y}f\left(\frac{y}{\hat{y}}\right) + (1 - \hat{y})f\left(\frac{1 - y}{1 - \hat{y}}\right).$$

Hence

$$\ell_f(1, \hat{y}) = \hat{y}f\left(\frac{1}{\hat{y}}\right) + (1 - \hat{y})f(0), \quad \ell_f(0, \hat{y}) = \hat{y}f(0) + (1 - \hat{y})f\left(\frac{1}{1 - \hat{y}}\right).$$

Set  $g(t) := f(t) - tf'(t)$ . Differentiating the induced binary loss gives

$$\frac{d}{d\hat{y}}\ell_f(1, \hat{y}) = g\left(\frac{1}{\hat{y}}\right) - f(0), \quad \frac{d}{d\hat{y}}\ell_f(0, \hat{y}) = f(0) - g\left(\frac{1}{1 - \hat{y}}\right).$$

By convexity, the tangent inequality at  $t > 0$ , evaluated at 0, gives

$$f(0) \geq f(t) + f'(t)(0 - t) = f(t) - tf'(t) = g(t).$$

Therefore  $g(1/\hat{y}) - f(0) \leq 0$  and  $f(0) - g(1/(1 - \hat{y})) \geq 0$ . Hence  $\hat{y} \mapsto \ell_f(1, \hat{y})$  is nonincreasing and  $\hat{y} \mapsto \ell_f(0, \hat{y})$  is nondecreasing. Thus,  $\ell_f$  is endpoint-monotone.  $\square$

## E Machine-Learning Details for Experiment 1

Experiment 1 illustrates the two-agent regression geometry from Proposition 4. The purpose of the experiment is to verify how the location of the constrained maximizer  $\alpha^*$  and the sign of complementarity depend on the angle and norm of the human–AI disagreement direction.

### E.1 Dataset and AI model

We use the California Housing regression dataset from `scikit-learn`. The target is the median house value of California districts expressed in hundreds of thousands of dollars (\$100,000). The data are split into training and test sets with a 75/25 split. The AI predictor is a random-forest regressor with 300 trees, `min_samples_leaf = 2`. No hyperparameter tuning is performed, because the model is used only to generate a fixed AI prediction vector  $\hat{y}^{AI}$ . Complementarity is computed on the held-out test set ( $n = 5160$ ), not on the training set. The resulting AI test RMSE is 0.5102, with

$$C_n = \|\hat{y}^{AI} - y\|_2^2 = 1343.2033 \quad ([\$100,000]^2).$$

#### E.1.1 Synthetic human predictions

Starting from the fixed test-set vectors  $y$  and  $\hat{y}^{AI}$ , we generate synthetic human predictions with controlled geometry. Let

$$e_1 = \frac{\hat{y}^{AI} - y}{\|\hat{y}^{AI} - y\|_2}.$$

We sample a random Gaussian vector, orthogonalize it against  $e_1$ , and normalize it to obtain a unit vector  $e_2$  with  $\langle e_1, e_2 \rangle \simeq 0$ . For a prescribed angle  $\theta$  and norm ratio  $q$ , the human–AI displacement is

$$\hat{y}^H - \hat{y}^{AI} = q\|\hat{y}^{AI} - y\|_2(\cos(\theta)e_1 + \sin(\theta)e_2),$$

so that

$$\angle(\hat{y}^H - \hat{y}^{AI}, \hat{y}^{AI} - y) = \theta, \quad \frac{\|\hat{y}^H - \hat{y}^{AI}\|_2}{\|\hat{y}^{AI} - y\|_2} = q.$$

The human prediction is then  $\hat{y}^H = \hat{y}^{AI} + (\hat{y}^H - \hat{y}^{AI})$ . This construction fixes the AI model and the test labels, while varying only the geometry of the synthetic human prediction.

## E.2 Complementarity computation

For each scenario, we compute  $A_n = \|\hat{y}^H - \hat{y}^{AI}\|_2^2$ ,  $B_n = \langle \hat{y}^H - \hat{y}^{AI}, \hat{y}^{AI} - y \rangle$ ,  $C_n = \|\hat{y}^{AI} - y\|_2^2$ , and the pointwise-oracle benchmark

$$nK_n = \sum_{i=1}^n \min\{(\hat{y}_i^H - y_i)^2, (\hat{y}_i^{AI} - y_i)^2\}.$$

For the linear team prediction  $\hat{y}_T(\alpha) = \alpha\hat{y}^H + (1 - \alpha)\hat{y}^{AI}$ ,  $\alpha \in [0, 1]$ , the plotted quantity is

$$n\Psi(\alpha) = -A_n\alpha^2 - 2B_n\alpha + (nK_n - C_n),$$

with constrained maximizer

$$\alpha^* = \Pi_{[0,1]}\left(-\frac{B_n}{A_n}\right).$$

## E.3 Scenarios

We evaluate five controlled scenarios:

$$(\theta, q) \in \{(0, 1.0), (\frac{\pi}{2}, 1.0), (\frac{3\pi}{4}, 0.5), (\frac{3\pi}{4}, 2.5), (\pi, 1.25)\}.$$

The first two scenarios test non-corrective and orthogonal human movement. The third is corrective but too short, so the unconstrained maximizer lies outside the feasible segment. The last two scenarios satisfy the interior condition and achieve positive complementarity. The  $\theta = \pi$  case is the collinear corrective case: the human–AI line passes through the ground-truth direction, so the geometric loss term proportional to  $\sin^2\theta$  vanishes.

## F Experiment 2 implementation details

We use the California Housing regression dataset with the same preprocessing, train–test split, and random forest model as in Experiment 1. A random forest regressor with 300 trees and `min_samples_leaf=2` is trained on the training set. All equality loci and performance quantities are computed on the held-out test set. Let  $\hat{y}^{AI}$  denote the AI prediction vector on the test set and let

$$r_{AI} := \hat{y}^{AI} - y$$

be the AI residual vector. We construct synthetic agent predictions in an AI-anchored geometry. For each synthetic agent  $j$ , let

$$d_j := \hat{y}^{(j)} - \hat{y}^{AI}$$

be its displacement from the AI prediction. We control the angle  $\theta_j = \angle(d_j, r_{AI})$  and the relative displacement size

$$q_j := \frac{\|\hat{y}^{(j)} - \hat{y}^{AI}\|_2}{\|\hat{y}^{AI} - y\|_2} = \frac{\|d_j\|_2}{\|r_{AI}\|_2}.$$

Thus, values  $\theta_j > 90^\circ$  indicate displacements that are corrective relative to the AI residual, whereas values  $\theta_j < 90^\circ$  move broadly in the same direction as the AI residual.

To generate the synthetic predictions, we draw a fixed unit vector  $u_\perp$  orthogonal to  $r_{AI}$  and set

$$\hat{y}^{(j)} = \hat{y}^{AI} + q_j \|r_{AI}\|_2 \left( \cos(\theta_j) \frac{r_{AI}}{\|r_{AI}\|_2} + \sin(\theta_j) u_\perp \right).$$

In all scenarios,  $\hat{y}^{(1)}$  is a fixed corrective expert with  $\theta_1 = 180^\circ$  and  $q_1 = 1.75$ , while  $\hat{y}^{(3)} = \hat{y}^{AI}$ . The assistant  $\hat{y}^{(2)}$  is varied across four regimes:

$$(\theta_2, q_2) \in \{(160^\circ, 0.50), (160^\circ, 1.50), (20^\circ, 0.50), (20^\circ, 1.50)\}.$$

These correspond respectively to weakly corrective, strongly corrective, weakly non-corrective, and strongly non-corrective assistant displacements relative to the AI residual.

For each scenario, we evaluate the two  $N = 3$  protocol trees  $T_L = ((12)3)$ ,  $T_R = (1(23))$ , with  $\hat{y}_{T_L}$  given by (18) and  $\hat{y}_{T_R}$  given by (19). The plotted quantity is the signed test-set MSE difference

$$\frac{P(\alpha_1, \alpha_2)}{n} = \frac{1}{n} (\|y - \hat{y}_{T_L}\|_2^2 - \|y - \hat{y}_{T_R}\|_2^2) = \text{MSE}(T_L) - \text{MSE}(T_R).$$

Hence  $P/n = 0$  is the protocol-indifference locus  $S_3$ ,  $P/n < 0$  indicates lower MSE for  $T_L$ , and  $P/n > 0$  indicates lower MSE for  $T_R$ . Here, lower tree MSE corresponds to higher complementarity value for that tree—see eq. (13). With the parameter convention in (18)–(19), the two root outputs satisfy  $\hat{y}_{T_L} - \hat{y}_{T_R} = \alpha_1(1 - \alpha_2)(\hat{y}^{(3)} - \hat{y}^{(1)})$ . Consequently,  $\alpha_1 = 0$  and  $\alpha_2 = 1$  are structural branches of  $S_3$  in every scenario. In the implementation,  $P/n$  is evaluated on a  $251 \times 251$  grid over  $[0, 1]^2$ .

## G Experiment 3 implementation details

Experiment 3 studies binary classification under cross-entropy and amplified logit pooling in the  $N = 2$  case. The goal is not to fit a real-data classifier, but to illustrate the mechanism by which leaving internality can make positive complementarity possible. We fix  $\alpha = 0.5$  and evaluate several amplification levels  $\lambda \in \{1, 2, 5, 10, 20\}$ .

We generate balanced  $n = 1000$  binary labels  $y_i \in \{0, 1\}$ , with  $I_1 = \{i : y_i = 1\}$  and  $I_0 = \{i : y_i = 0\}$ . For each simulated pair of probabilistic predictors, the construction is performed in logit space. Let  $s_i := 2y_i - 1 \in \{-1, 1\}$ . We first generate a midpoint logit  $C_i$ , which is the unamplified pooled logit for  $\alpha = \frac{1}{2}$ . Its magnitude is sampled around a dataset-level signal-strength parameter, while its sign is  $s_i$  except for a randomly flipped fraction of observations. Thus most pooled logits point toward the correct class, while a controlled fraction points in the wrong direction, meaning that amplification pushes the output opposite to the locally complementary direction: toward class 0 on  $I_1$ , or toward class 1 on  $I_0$ . The two agent logits are then placed symmetrically around this midpoint as  $z_i^{(1)} = C_i + \delta_i/2$  and  $z_i^{(2)} = C_i - \delta_i/2$ , where  $\delta_i$  is Gaussian disagreement noise. The resulting probabilities are  $\hat{y}_i^{(1)} = \sigma(z_i^{(1)})$  and  $\hat{y}_i^{(2)} = \sigma(z_i^{(2)})$ .

For a fixed  $\lambda$ , the amplified logit-pooling output is  $m_{2, \frac{1}{2}, \lambda}^{\text{logit}}(\hat{y}_i^{(1)}, \hat{y}_i^{(2)}) = \sigma(\lambda C_i)$ , since  $\alpha = \frac{1}{2}$ .

We also compute the class-wise rates of canonical local complementarity. On  $I_1$ , we define  $k_1$  as the fraction of observations satisfying  $m_{2, \frac{1}{2}, \lambda}^{\text{logit}}(\hat{y}_i^{(1)}, \hat{y}_i^{(2)}) > \max\{\hat{y}_i^{(1)}, \hat{y}_i^{(2)}\}$ . On  $I_0$ , we define  $k_0$  as the fraction satisfying  $m_{2, \frac{1}{2}, \lambda}^{\text{logit}}(\hat{y}_i^{(1)}, \hat{y}_i^{(2)}) < \min\{\hat{y}_i^{(1)}, \hat{y}_i^{(2)}\}$ . These are the local cases in which the amplified output leaves the interval spanned by the two input probabilities in the direction of the true class. For  $\lambda = 1$ , ordinary logit pooling is internal, so these strict outside-interval conditions cannot occur. For  $\lambda > 1$ , amplification may create such cases by moving the pooled logit away from 0, toward class 1 if  $C_i > 0$  and toward class 0 if  $C_i < 0$ . We finalize the experiment computing the complementarity functional (2) using binary cross-entropy as loss function.

## References

- Syed Mumtaz Ali and Samuel D Silvey. A general class of coefficients of divergence of one distribution from another. *Journal of the Royal Statistical Society: Series B (Methodological)*, 28(1):131–142, 1966.
- Gagan Bansal, Besmira Nushi, Ece Kamar, Eric Horvitz, and Daniel S Weld. Is the most accurate AI the best teammate? Optimizing ai for teamwork. In *Proceedings of the AAAI Conference on Artificial Intelligence*, volume 35, pages 11405–11414, 2021a.
- Gagan Bansal, Tongshuang Wu, Joyce Zhou, Raymond Fok, Besmira Nushi, Ece Kamar, Marco Tulio Ribeiro, and Daniel Weld. Does the whole exceed its parts? The effect of AI explanations on complementary team performance. In *Proceedings of the 2021 CHI conference on human factors in computing systems*, pages 1–16, 2021b.
- Lev M Bregman. The relaxation method of finding the common point of convex sets and its application to the solution of problems in convex programming. *USSR Computational Mathematics and Mathematical Physics*, 7(3):200–217, 1967.
- Kate Donahue, Alexandra Chouldechova, and Krishnaram Kenthapadi. Human-algorithm collaboration: Achieving complementarity and avoiding unfairness. In *Proceedings of the 2022 ACM Conference on Fairness, Accountability, and Transparency*, pages 1639–1656, 2022.

- Andrea Ferrario. Being pragmatic about reliance and trust in artificial intelligence. *Minds and Machines*, 36(1):5, 2025.
- Andrea Ferrario, Alessandro Facchini, and Juan M Durán. Epistemology gives a future to complementarity in human-AI interactions. *arXiv preprint arXiv:2601.09871*, 2026.
- Shigeru Furuichi, Kenjiro Yanagi, and Ken Kuriyama. Fundamental properties of Tsallis relative entropy. *Journal of Mathematical Physics*, 45(12):4868–4877, 2004.
- Patrick Hemmer, Max Schemmer, Michael Vössing, and Niklas Kühl. Human-AI complementarity in hybrid intelligence systems: A structured literature review. *PACIS*, 78, 2021.
- Patrick Hemmer, Sebastian Schellhammer, Michael Vössing, Johannes Jakubik, and Gerhard Satzger. Forming effective human-AI teams: Building machine learning models that complement the capabilities of multiple experts. In *Proceedings of the Thirty-First International Joint Conference on Artificial Intelligence*, pages 2478–2484, 2022.
- Philipp Hemmer, Michael Schemmer, Niklas Kühl, Maximilian Vössing, and Gerhard Satzger. Complementarity in human-AI collaboration: Concept, sources, and evidence. *European Journal of Information Systems*, pages 1–24, 2025.
- Andrey Kolmogorov. On the notion of mean. *Mathematics and Mechanics*, 199(1):144–146, 1930.
- Tim Miller. Explainable AI is dead, long live explainable AI! Hypothesis-driven decision support using evaluative AI. In *Proceedings of the 2023 ACM Conference on Fairness, Accountability, and Transparency*, pages 333–342, 2023.
- Mitio Nagumo. Über eine Klasse der Mittelwerte. In *Japanese Journal of Mathematics: Transactions and Abstracts*, volume 7, pages 71–79. The Mathematical Society of Japan, 1930.
- Eric Neyman and Tim Roughgarden. No-regret learning with unbounded losses: The case of logarithmic pooling. *Advances in Neural Information Processing Systems*, 36:21857–21877, 2023a.
- Eric Neyman and Tim Roughgarden. From proper scoring rules to max-min optimal forecast aggregation. *Operations Research*, 71(6):2175–2195, 2023b.
- Helbert Paat and Guohao Shen. Conformal set-based human-AI complementarity with multiple experts. *arXiv preprint arXiv:2508.06997*, 2025.
- Kenny Peng, Nikhil Garg, and Jon Kleinberg. A no free lunch theorem for human-AI collaboration. In *Proceedings of the AAAI Conference on Artificial Intelligence*, volume 39, pages 14369–14376, 2025.
- Charvi Rastogi, Liu Leqi, Kenneth Holstein, and Hoda Heidari. A taxonomy of human and ml strengths in decision-making to investigate human-ML complementarity. In *Proceedings of the AAAI Conference on Human Computation and Crowdsourcing*, volume 11, pages 127–139, 2023.
- Max Schemmer, Niklas Kuehl, Carina Benz, Andrea Bartos, and Gerhard Satzger. Appropriate reliance on AI advice: Conceptualization and the effect of explanations. In *Proceedings of the 28th International Conference on Intelligent User Interfaces*, IUI '23, page 410–422, New York, NY, USA, 2023. Association for Computing Machinery.
- James Dillon Stasheff. Homotopy associativity of H-spaces. I. *Transactions of the American Mathematical Society*, 108(2):275–292, August 1963.
- Dov Tamari. Problèmes d’associativité des monoïdes et problèmes des mots pour les groupes. *Séminaire Dubreil. Algèbre et théorie des nombres*, 16(1):1–29, 1962.
- Constantino Tsallis. Possible generalization of Boltzmann-Gibbs statistics. *Journal of Statistical Physics*, 52(1): 479–487, 1988.
- Michelle Vaccaro, Abdullah Almaatouq, and Thomas Malone. When combinations of humans and AI are useful: A systematic review and meta-analysis. *Nature Human Behaviour*, 8(12):2293–2303, 2024.
- Rajeev Verma, Daniel Barrejón, and Eric Nalisnick. Learning to defer to multiple experts: Consistent surrogate losses, confidence calibration, and conformal ensembles. In *International Conference on Artificial Intelligence and Statistics*, pages 11415–11434. PMLR, 2023.
- Noson S Yanofsky. *Monoidal Category Theory: Unifying Concepts in Mathematics, Physics, and Computing*. MIT Press, 2024.
- Yunfeng Zhang, Q Vera Liao, and Rachel KE Bellamy. Effect of confidence and explanation on accuracy and trust calibration in AI-assisted decision making. In *Proceedings of the 2020 Conference on Fairness, Accountability, and Transparency*, pages 295–305, 2020.